Characterization of Conductive Self-healing Protein Materials

By Saadia Wasim

Department of Chemical Engineering

McGill University, Montreal

December 2019

A thesis submitted to McGill University in partial fulfillment of the requirements of the degree of Master of Engineering

© Saadia Wasim 2019

Abstract

With the development of electronic technologies, and their emerging use in the fields of biomedicine and bio-interfaces, there is a need for greener alternative materials which can be sustainable for the environment and non-toxic. The use of self-healing conductive protein materials in bio-electronics could revolutionize the field as they exhibit several advantages over conventional semiconductors; they are biodegradable, biocompatible, flexible and can be genetically engineered. Here, we aim at characterizing and studying the material's properties of engineered curli protein nanofibers produced by *E. coli* bacteria. These fibers were engineered to contain a high density of tryptophan residues, an aromatic amino acid, to mimic the conductivity mechanism observed in the naturally-conductive bacteria, *Geobacter sulfurreducens*. To confirm π-orbital overlap for electron delocalization, the effect of pH and the beta-sheet folded conformation of the proteins; fluorescence, Raman spectroscopy and circular dichroism measurements were performed. Next, electrical characterization was performed to study the effect of factors on conductance such as thickness and drying of the film. It was observed that charge transport is both a surface and bulk phenomenon as a direct relationship between conductance and thickness was established. Moreover, humidity was found to play an important role in maintaining the protein configuration for the charges to flow. Furthermore, the desirable self-healing nature of the protein fibers was also examined via microscopy and electrical measurements, for applications as flexible and stretchable materials. Successful electrical healing with more than 95% recovery of conductivity for Trp1 mutant thin film was observed with the use of water, suggesting that they can potentially be used as self-healing humidity sensors.

Sommaire

Avec le développement de technologies électroniques et leur utilisation émergente en biomédecine et en bio-interfaces, il y a un besoin pour des matériaux alternatifs verts soutenables pour l'environnement et non-toxiques. L'utilisation de matériaux à partir de protéines conductives et auto-régénératrices pourra révolutionner le domaine puisque ces protéines démontrent plusieurs avantages comparés aux semiconducteurs conventionnels; elles sont biodégradables, biocompatibles, souples et peuvent être modifiées génétiquement. Dans ce document, nous cherchons à caractériser et étudier les propriétés de nanofibres de protéines curli génétiquement modifiées produites par la bactérie *E. coli*. Ces fibres ont été modifiées génétiquement pour exprimer une plus haute densité de résidus de tryptophane, un acide aminé, pour imiter le mécanisme de conductivité observé chez la bactérie naturellement conductive, *Geobacter sulfurreducens*. Afin de confirmer le recouvrement de liaisons π qui crée une délocalisation d'électrons, l'effet du pH et la conformation de feuillets bêta de la protéine pliée, la fluorescence, la spectroscopie de Raman et le dichroïsme circulaire ont été exécutés. Ensuite, la caractérisation électronique a été réalisée afin d'étudier l'effet de facteurs sur la conductance tel l'épaisseur et le taux d'humidité du film. Le transport de charge a été observé à la surface et à l'intérieur du matériel, puisqu'une relation directe entre l'épaisseur du film et la conductance a été établie. De plus, l'humidité a été démontrée de jouer un rôle dans la conservation de la structure de la protéine pour permettre le flux de charges. La qualité auto-régénératrice des fibres de protéines a aussi été examinée par microscopie et par quantification électrique, pour être utilisées en tant que matériaux souples et flexibles. La conductivité électrique a été rétablie avec plus de 95% d'efficacité pour un film à partir du mutant Trp1 à l'aide d'une goutte d'eau, ce qui suggère l'application potentielle de ces films comme capteurs d'humidité auto-réparateurs.

Acknowledgements

I would like to thank my thesis supervisor, Prof. Noémie-Manuelle Dorval Courchesne, of Department of Chemical Engineering at McGill University for giving me the opportunity to be her first M.Eng. student, for giving importance to our opinions and involving us in the lab setup, for giving me the opportunity to experience the development of the lab from scratch, for making me her first safety officer, and many more. But, most importantly for supporting, showing patience and being unbiased. She has helped me not only enhance my knowledge and finish this thesis with quality/quantity of work yet making this my work, but also helped me stay strong. Moreover, I would like to highly appreciate my department for considering me a recipient of EUL scholarship.

I would also like to thank my lab members for all their help and memories that added quality to my education. I would also like to thank our technical staff (Andrew, Lou, Ranjan) for immediate help with the instruments, Frank for his guidance to comply by the rules as a safety officer and non-technical staff (Ms. Louise and Ms. Anna) for answering questions related to my program.

I have no words to express my gratitude for my parents and siblings for keeping me motivated and grounded in every situation. I would specifically like to thank my mother and grandmother for their support in the form of blessings which helped me come so far in life and way to go. Their respect for education has been my driving force in all my academic achievements so far. I would also like to thank my father for always motivating me and my siblings for all the wonderful memories we share. I would also like to thank two of my dear friends, Pooja and Nidhi, for there support.

Contribution of Authors

Saadia Wasim performed the experimental work, data analysis and writing tasks with the exceptions of those mentioned below. Dr. Noemie-Manuelle Dorval Courchesne helped structure the project, provided general guidance throughout the project, and reviewed all the chapters of this thesis. The fluorescence spectroscopy measurements were performed in the Tufenkji Lab. The work performed in Chapter 3 serves as ground for a journal article, which will be co-authored by two other members of the Dorval Lab, Daniel Modafferi and Sophia Roy. They helped in obtaining the three optical microscope images in Figure 4.7 and the I-V graph for Trp1 mutant in Figure 4.8.

Table of Contents

List of Figures

List of Tables

Chapter 1 : Introduction

1.1. Electronic Waste: a threat to the Environment

In this fast-developing world, we are increasingly becoming dependant on electronics. Everything around us in our everyday life is directly or indirectly connected with technology, such as solar cells, sensors, processors, electronic circuits, light emitting diodes, etc. These fast-technological developments are the result of the revolution in electronics where inorganic semiconductors like gallium arsenide and silicon take the lead. With the growing demands from the consumers, a wide range of technological varieties are manufactured, which results in high energy consumption during the manufacturing process. Even though electronics have become more efficient with time, there is an energy imbalance between energy consumed during manufacturing and energy consumed during the lifetime of the product. The energy consumed during the manufacturing process of nanomaterials (carbon nanotubes, nanofibers) used in electronics or inorganic semiconductors (high grade silicon) is six or more orders of magnitude than compared to the energy required for plastics or metals like aluminium, iron, etc[1]. One way of achieving sustainability in the electronics industry is by using materials that consume less energy during the manufacturing stage[2].

Rapid changes in technologies, resulting in an increased electronics demand, are not just causing an energy imbalance but also causing replacement of the old electronics with new ones, thereby resulting in huge quantities of electronic waste (e-waste) and consumption of scarce natural resources like indium and gallium. About 50 million tonnes of e-waste, which includes all electrical and electronic wastes, was predicted to be generated worldwide in 2018[3]. The United States of America, the European Union, Japan, and China are the leading e-waste contributors, and

developing countries like Nigeria, India, Pakistan, and Ghana are the main importing nations in the world. The majority of e-waste is either incinerated or dumped into landfills, and a fraction of it is sent for recycling. There are many negative consequences of incineration and landfill treatment such as mercury emission, greenhouse gas emissions, realize of dioxins upon incineration of PVC and leaching of toxic chemicals and metals into the soil resulting in soil pollution[4]. Apart from the negative consequences, e-waste treatment in state-of-the-art facilities is limited in most nations, as they still lag e-waste management systems and therefore, these wastes are not being taken care of. Furthermore, some developed countries ship their e-waste to developing countries where inefficient techniques are being used which can be dangerous for the environment and the well being of the workers involved. Therefore, there is a stressing need to shift our resource consumption from non-renewable resources to renewable resources and manage e-waste disposal efficiently in order to protect the environment for a sustainable future[4].

To overcome the negative consequences of these huge quantities of e-waste, the use of polymers in devices is emerging. Inorganic semiconductors are not just expensive; but also, non-biodegradable and obtained from non-renewable resources, thereby making them non-sustainable. Therefore, there is a need for a "Green" solution which is environmentally friendly. Organic polymers are replacing inorganic semiconductors due to their low cost, easy to fabrication and more flexible product compared to inorganic semiconductors. Some of their applications include organic solar cell (OSC), organic field effect transistor (OFET), organic light emitting diode (OLED), and organic vapor phase deposition (OVPD). However, the source of production makes most organic polymers not sustainable for the environment and for practical uses. Organic polymers are produced from non-renewable resources, therefore, even if they are biodegradable, they still require production processes that may be harmful for the environment. Therefore, the

use of proteins obtained from renewable resources in bio-electronics is of growing interest. The use of proteins in the development of electronic devices resulted in a new field of science called proteotronics in 2014[5]. Proteins are made up of twenty different types building blocks called amino acids. Proteins can change their tertiary structure from a native state to activated state due to an external stimulus. This response to an external stimulus makes proteins interesting candidates for nano-scale bio-sensing applications. For example, a transmembrane protein, bovine rhodopsin, is light sensitive and changes structure upon activation. This structural change is then biologically communicated internally to the chimpanzee OR-7D4, an olfactory receptor, which changes color upon activation from purple to green[6]. The sensing ability of proteins makes them an excellent example of mini sensors. We are interested in using conductive proteins in the fabrication of electronic devices such as wearable and flexible biosensors. Compared to most of the proteins studied by researchers, the protein of our interest is not just sustainable but can be produced in large quantities and most importantly can be genetically manipulated for the development of different types of sensors[7].

Chapter 2 : Literature Review

2.1. Conductive Proteins as a Sustainable Alternative Solution

Electrically conductive protein nanowires produced as extracellular appendages from micro-organisms are of growing interest because they can serve as a channel for long-range electron transport. These conductive nanowires are sustainably produced (biosynthesized) and can be used in a wide range of applications. The structure of these conductive proteins is being studied to gain insight into the charge transfer mechanism leading to long-range conductivity. Studies performed on proteins show that the presence of aromatic amino acids plays a key role in long-range electron transfer. Possibly, the presence of the conjugated bonds in the aromatic rings helps in the delocalization of electrons via π-π stacking.

Examples of tryptophan-containing peptides and proteins that exhibit electronic conductivity are shown in Figure 2.1. The conductivity of tryptophan-containing proteins was first investigated by Amdursky using small self-assembling peptides. They observed that peptide nanodot (PND) composed of phenylalanine-tryptophan dipeptides had 5-fold higher conductivity than phenylalanine-phenylalanine dipeptides using conductive probe atomic force microscopy (Figure 2.1 a)[8]. Another example for electron delocalization in a peptide is the self-assembled eight-residue cyclic D, L-α-peptide. It is composed of diimide side chains which helps in delocalizing electrons up to hundreds of nm (Figure 2.1 b)[9].

Naturally produced conductive protein nanowires can be found in nature. One of the examples include, an electrically conductive protein nanowire, produced by the bacterium *Methanospirillum hungatei*. Proteins forming this nanowire contain several phenylalanine residues in their hydrophobic core, organized together to form the route for electron transfer (Figure 2.1

c)[10]. Another example of naturally conductive nanowires include pili proteins secreted by *Geobacter sulfurreducens* have aromatic residues in the exterior of the α-helical structure[11,12] as shown in Figure 2.1 d to facilitate electron transfer.

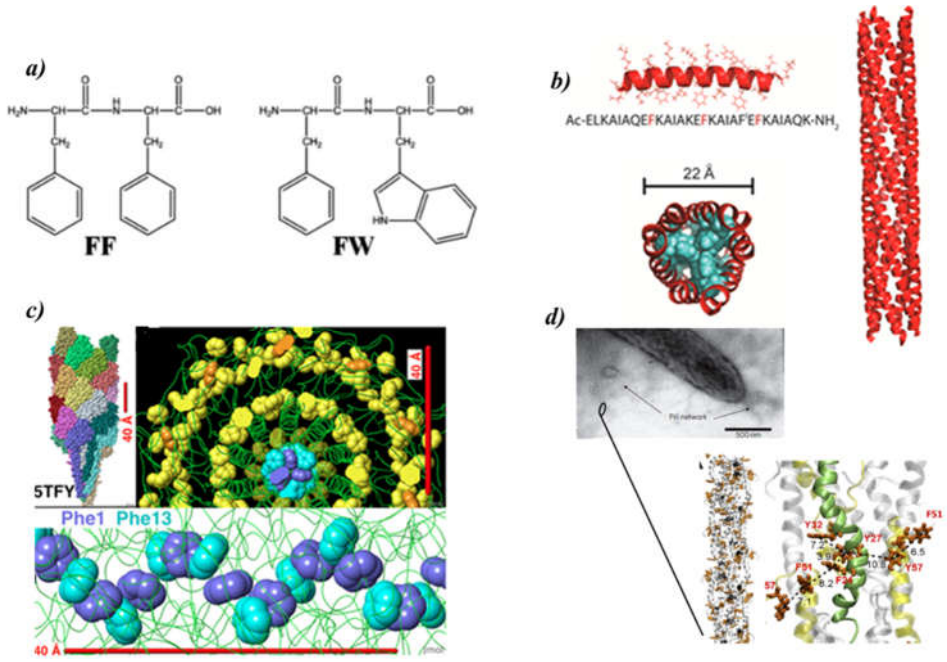

Figure 2.1. Natural and synthetic proteins with aromatic amino acids, a) tryptophan containing small peptides[8], b) α-helical dipeptides containing phenylalanine residues[9], c) *M. hungatei* containing phenylalanine residues in the hydrophobic core[10], and d) pili fibers containing phenylalanine and tyrosine residues[11,12].

PilA, a protein monomer, is secreted by *Geobacter* species in the extracellular matrix self-assembles to form conductive protein fibers called pili[13,14]. The conductivity of these protein fibers can be tuned by modifying the number of aromatic amino acid residues in *pilA* gene. For example, synthetic W51W57 pili have higher conductivity than wild-type pili due to the presence of aromatic amino acids (tryptophan) on the 51st and 57th position of the pili fiber[15]. Experiments conducted on *Geobacter sulfurreducens* showed that the protein-rich pili fibers were able to conduct electrons over μm distances and network of pili fibers could conduct over centimeter distances, resembling metallic-like conductivity[16,17]. Previous studies discuss that the metallic-like

conductivity in PilA can be due to the overlapping π-orbital of the aromatic amino acids [16,18] and interactions between the aromatic amino acids with a spacing of 3.2 Å[19]. This short spacing between the aromatic amino acids allows for effective π-orbital overlapping and electron delocalization[16,19]. The conductivity of wild-type pili (conductivity values) is in the same order of magnitude as the conductivity of polypyrrole (0.91 mS cm^{-1})[20] and PEDOT (90-600 mS cm^{-1})[21], as shown in Figure 2.2.

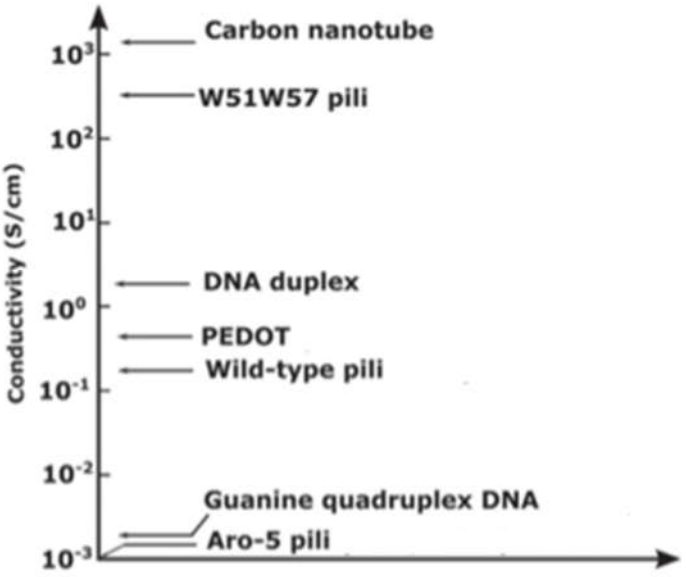

Figure 2.2.Comparison of conductivities of organic nanowires of similar diameter[15].

The expression of the *pilA* gene of *G. metallireducens,* a gram-negative proteobacterium, in *G. sulfurreducens* resulted in pili fibers that had high conductivity due to the presence of aromatic residues. *G. metallireducens* contains aromatic residues such as tyrosine, histidine and phenylalanine at different positions where there are non-aromatic residues located in *G. sulfurreducens.* Therefore, the increase in conductivity was attributed to the excess aromatic residues.

2.1.1. Curli Nanofiber Proteins

Here, we are specifically interested in a type of amyloid fibers, curli nanofibers, which are naturally produced and secreted in the extracellular matrix of bacteria *Escherichia coli* and *Salmonella enterica*[22]. Curli nanofibers unlike pili proteins (secreted from geobacter species) are economical as their production can be easily scaled-up[23]. These curli nanofibers remain functional throughout their processing and are highly resistant to detergents, heat, solvents and denaturing agents[24]. Curli nanofibers have gained interest for producing genetically engineered materials since *E. coli* can be easily engineered to produce recombinant proteins. The fibers can be genetically engineered either by introducing site-specific mutation within the core of the main curli subunit, or by adding a functional protein domain at the C-terminal of the main curli subunit. Curli-based materials are useful for applications in electronically conductive materials, biocatalysts and custom fabricated surface coating[23].

2.1.1.1. Secretion and Self-Assembly of Curli Fibers

Curli nanofibers are secreted into the extracellular matrix of *E. coli* bacteria. There are seven curli specific genes (*csgA*, *csgB*, *csgC*, *csgD*, *csgE*, *csgF*, and *csgG*) involved in the expression and self-assembly of curli nanofibers[25] (Figure 2.3). Each curli gene has a specific role to perform during the secretion pathway as follows:

1) CsgA: Mediates structure, self-assembles into curli fibers
2) CsgB: Starts nucleation of CsgA fibers
3) CsgC: Prevents CsgA and CsgB from forming polymers
4) CsgD: Direct transcription regulator
5) CsgE and CsgF: Periplasmic proteins helps in processing by interacting with CsgG

6) CsgG: Outer membrane protein which helps in the secretion and stability of CsgA and B

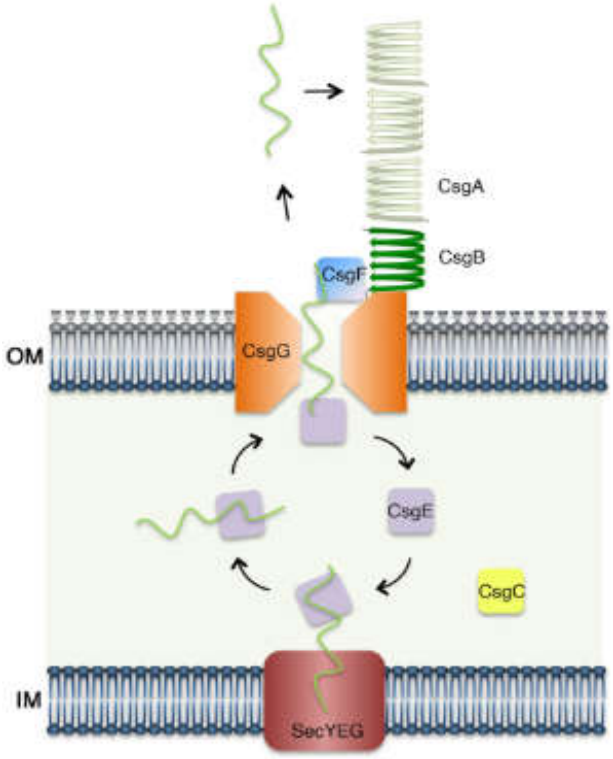

Figure 2.3. Schematic representation of secretion and self-assembly of curli nanofibers from the inner membrane and outer membrane to the exterior of an *E.coli* cell[25].

2.1.1.2. Scalability of Curli Fibers through Filtration

Conventional purification techniques for recombinant proteins include centrifugation, salt precipitation, affinity chromatography or SDS-PAGE[26–28]. The yield through these techniques is usually very low and likely to be in milligrams or sub milligrams[23]. To produce enough curli nanofibers to make gels, films or functional materials, a simpler, faster and high yielding method was needed. Filtration is a faster and simpler way of isolating the amyloid proteins from the biofilm. It is a size dependent technique and therefore, useful for separating curli fiber aggregates from the bacterial cells in the culture (Figure 2.4). The bacterial cultures are filtered and washed with several readily available reagents, such as guanidium chloride, sodium dodecyl sulphate, and

nuclease to yield purified amyloid proteins. There are several advantages of using filtration technique for the purification of curli nanofibers, such as it can be scaled up to purify several liters of bacterial cultures, it does not rely on binding affinity, it does not require protein tags, and it can be used to purify genetically engineered proteins. Curli fibers can be a part of the biofilm attached to the surface of the cells in the extracellular matrix or separated from the cell surface through purification technique such as filtration[23].

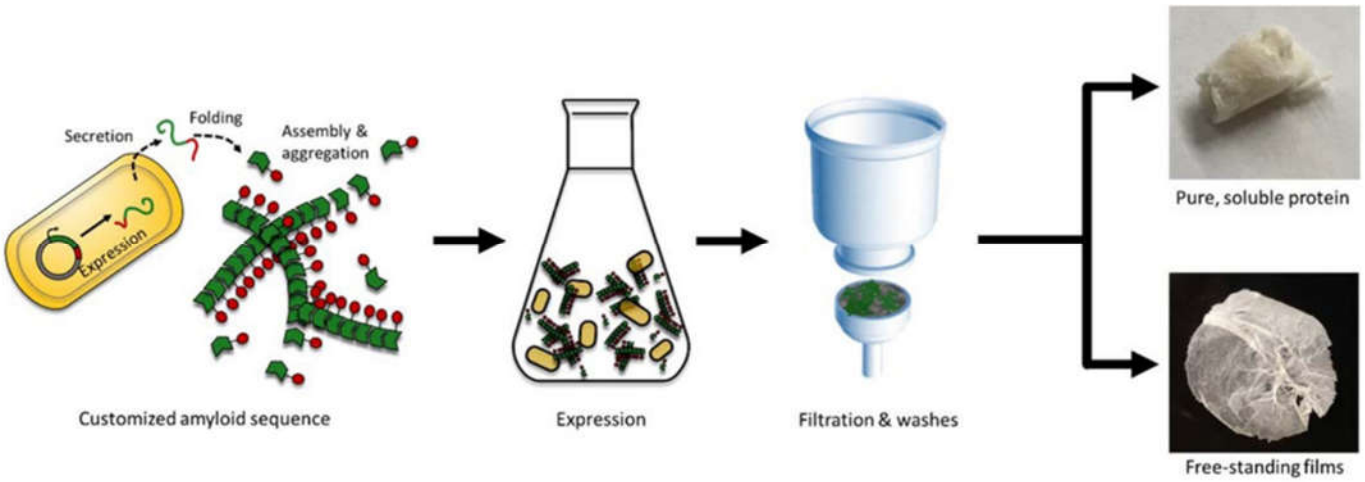

Figure 2.4: Schematic representation of steps involved in obtaining curli nanofiber free standing thin films and lyophilized fibers[23].

2.1.1.3. Engineered Conductivity in Curli fibers

In order to render curli nanofibers conductive, mutations on the exterior residues of the CsgA were previously performed to closely position the aromatic rings for the transport of electrons through π-stacking[7]. It was suggested that if electron transfer can occur within a single CsgA protein, then it can occur along a fully assembled curli nanofibers for long-range electron transport.

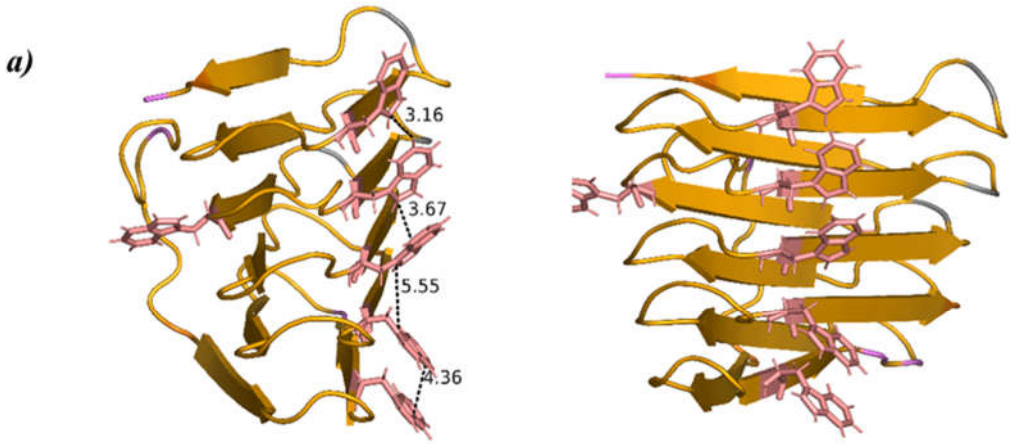

b)

22	24	26	28	30	35	37	39	41
Asn	Glu	Asn	Tyr	Tyr	Ser	Leu	Leu	Thr
45	47	49	51	53	58	60	62	64
Asn	Asp	Thr	Thr	His	Gly	Asp	Gly	Gly
67	69	71	73	75	80	82	84	86
Asp	Ser	Asp	Thr	Arg	Ser	Thr	Asp	Trp
90	92	94	96	98	103	105	107	109
Asn	Glu	Thr	Lys	Phe	Gly	Ala	Asp	Thr
112	114	116	118	120	125	127	129	131
Asn	Ser	Asn	Thr	Val	Asn	Thr	His	Tyr

Figure 2.5. a) Side view of rows closest spacing for Trp1 mutant is 3.16 Å, furthest is 5.55 Å, and front view (right) of the aromatic residues genetically incorporated into the protein, b) wild-type sequence of amino acids in CsgA monomer for the rows 1,2,3,4, and 5 used for mutations. The numbers denote the position of mutation in the CsgA monomer and the colored boxes denote the charges of the amino acid residues. Red amino acids denote negatively charged residues and blue denote positively charged residues[7].

Mutations on rows 1, 2, 3, 4, and 5 were performed with different aromatic amino acids (Figure 2.5 b). From Figure 2.6, it can be observed that the first stack was genetically modified with different aromatic amino acid residues, and the mutants were labeled with the aromatic amino acid introduced and the number of the row mutated, e.g. for row 1: Trp1, Tyr1, His1, Phe1, and all rows Trp for a protein with all rows mutated simultaneously. These residues carry different charges, for instance, Tyr has oxidizable phenol group which can respond to varying pH, His is a

positive amino acid, and Phe and Trp are neutral hydrophobic aromatic amino acids which can act as a mediator for an easy flow of electrons. The charged amino acids can be a medium for conducting charges across the protein fiber. Mutations were performed to satisfy three criteria; firstly, the residue group should face outwards to ensure CsgA stability; secondly, these groups were on the exterior of the β-sheet structure of the CsgA monomer; and thirdly, these residues were aligned in such a way that they would form a continuous array of aromatic rings with a spacing of 5 to 6.5 Å (Figure 2.5 a). Analysis of the inter-residue interactions and stability of the mutants were performed using molecular dynamics and quantum mechanics simulations. It was observed that all the mutant CsgA were stable as the average position of the overlapping values were under 2 Å.

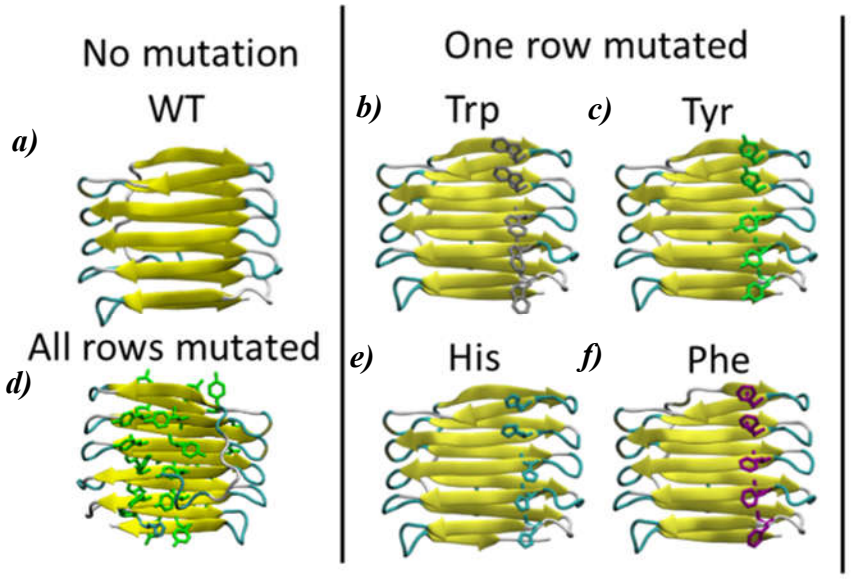

Figure 2.6. Site-specific mutations performed on CsgA, a) WT with no mutation, b) Trp1: WT mutated with five tryptophan residues on stack 1, c) Tyr1: WT mutated with five tyrosine residues on stack 1, d) All stack Tyr: WT mutated with twenty-five tyrosine residues from 1-5 stacks, e) His1: WT mutated with five histidine residues on stack 1, f) Phe1: WT mutated with five phenylalanine residues on stack 1[7].

2.1.2. Conductivity Mechanism in Proteins Containing Aromatic Residues

Proteins can demonstrate two possible conductivity mechanisms, electron delocalization and hopping. In metallic-like conduction mechanism, charges are spread across the site and require enough band gap energy for the charges (electrons) to flow (Figure 2.7 a). In proteins and peptides, the band gaps range from ≤ 4 eV semiconducting to > 4 eV insulating[29–31]. The band gap energy can be decreased by incorporating aromatic amino acid residues to help in the delocalization of electrons via π-orbital overlap, also known as π-π stacking. This overlap of the orbitals results in delocalized states, due to the distance between the aromatic residues (less than 5 Å). π- π stacking results in metallic-like or semiconductor like behavior due to the delocalized electron transport in conductive organic polymers. Similar phenomena can also occur in proteins and peptides if they fulfill the required two criteria: 1) they contain aromatic residues that can form π- π stacking with long-range periodicity, and 2) the distance between the adjacent aromatic residues is sufficiently small to allow for electron delocalization. In hopping mechanism, charges move from one site to the next and are localized to each site (Figure 2.7 b). If the electron delocalization across the electrode gets interrupted due to insufficient π- π stacking, i.e., if the aromatic rings are far apart,

then thermally activated hopping becomes the dominant conductivity mechanism[32,33].

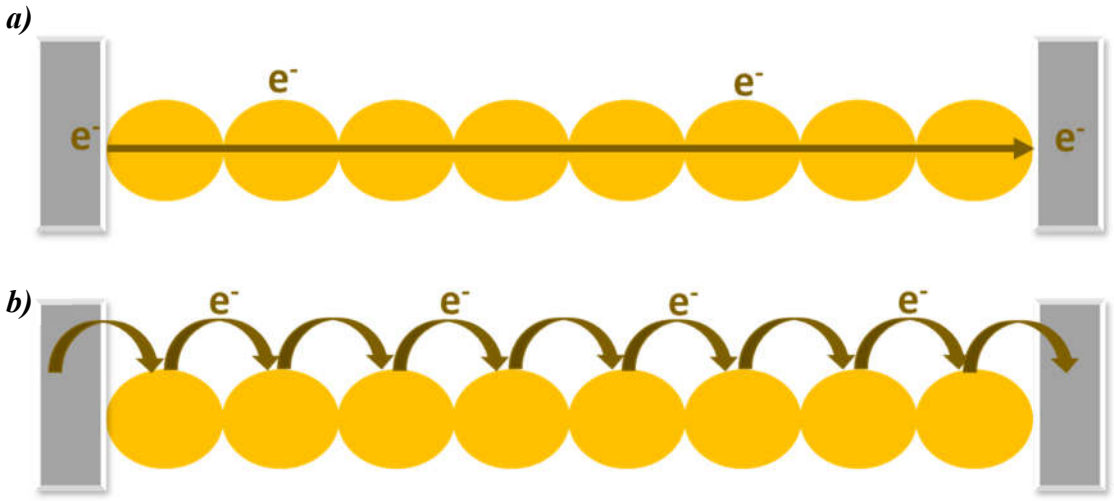

Figure 2.7. Schematic representation of the two main conduction mechanisms in proteins a) electron delocalization via π-stacking, b) hopping across the filament.

2.1.2.1. Fluorescence as a Tool to Understand Interactions between Aromatic Residues

Fluorescence is a spectroscopic technique used to analyze fluorescence properties of samples. It involves the absorption of a photon of a specific energy by an electron in a molecule. After a relaxation step to a lower electronic state, the electron returns to the ground state, which emits a photon of lower energy than that absorbed. Proteins are known to display a unique intrinsic fluorescence. Three aromatic amino acids, Trp, Tyr, Phe, have intrinsically ultra-violet fluorescence (Table 2.1). Amongst the three aromatic amino acids, tryptophan dominates the emission of the proteins. It has the largest extinction coefficient and absorbs at the longest wavelength. However, a protein possesses only one or a few tryptophan residues which helps in spectral data interpretation[34].

Emission from each tryptophan residue depends on the environment. Tryptophan in water has an emission max at 350 nm and is highly sensitive to the polarity of the solvent or the local

environment. In non-polar solvents, tryptophan residues show a blue-shifted spectrum (to lower wavelength)[34]. Tryptophan can be excited at 295 nm to 305 nm to avoid the excitation of tyrosine and minimize the excitation of phenylalanine residues. Therefore, most experiments use 295 nm to excite tryptophan residues in the protein[34].

Resonance energy transfer (RET) also known as fluorescence resonance energy transfer (FRET) occurs between two molecules a donor and an acceptor, with a spectral overlap between the donor's emission and the acceptor's excitation (Figure 2.8). Energy can be transferred non-radiatively from the excited donor to the acceptor. The observed emission spectrum will be the spectrum of the acceptor. RET has been observed amongst the aromatic amino acids in a protein. RET occurs from phenylalanine to tyrosine to tryptophan because of their spectral properties. This is the reason for the small contribution of phenylalanine and tyrosine to the emission of proteins.

Table 2.1. Absorption and Fluorescence wavelength for different aromatic amino acids

Aromatic residues	Absorption Wavelength (nm)	Fluorescence Wavelength (nm)
Tryptophan	280	348
Tyrosine	274	303
Phenylalanine	257	282

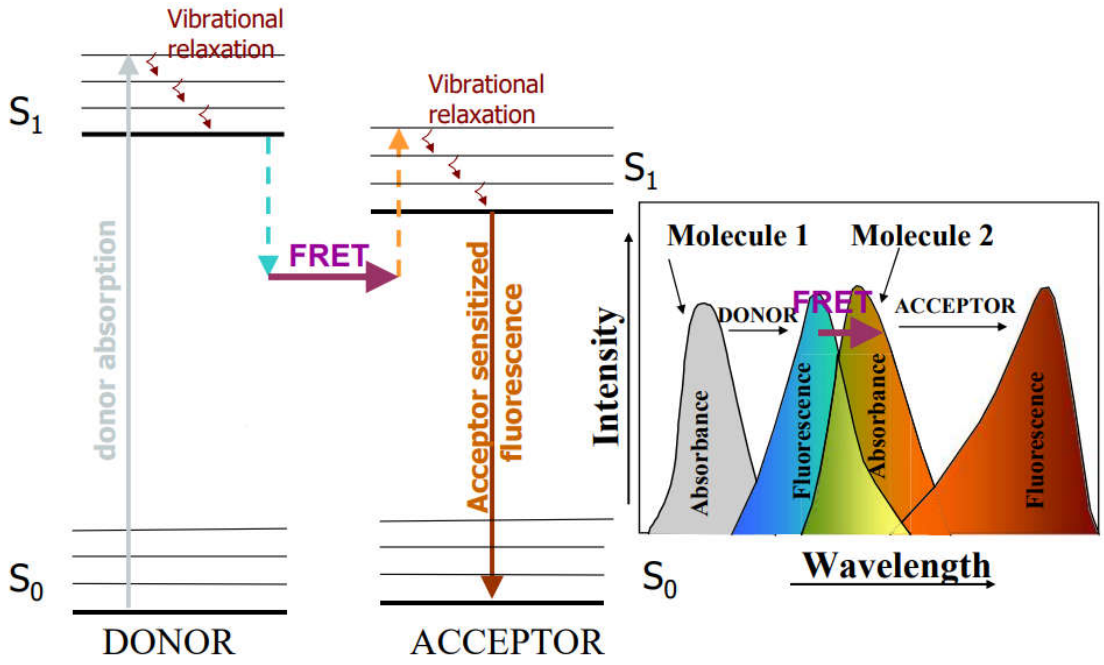

Figure 2.8. Schematic representation of FRET between two molecules due to their spectral overlap resulting in energy transfer from donor molecule to acceptor molecule[34]

In a protein that contains several tryptophan residues, each tryptophan has its own share of contribution to the emission spectrum. Tryptophan emission spectrum reflects the environment of the tryptophan residues. When tryptophan residues are in non-polar environment (located in the hydrophobic core of the protein or trapped in a hydrophobic aggregate), a blue shifted peak is observed (to shorter wavelengths). When they are in polar environment, exposed to water or when they become hydrogen-bonded, a red-shift is observed (to longer wavelengths). For example, azurin (a tetrameric protein made up of 128 amino acids) has a shielded tryptophan residue in the hydrophobic core, therefore it displays a blue shift while adrenocorticotropin hormone (ACTH) has emission max of an exposed tryptophan at around 350 nm. Therefore, the environment of our proteins can be investigated from the spectral peak of the emission scan. Protein fluorescence,

therefore, can be used to study protein dynamics, functions and structure such as protein folding[34–36].

π-stacking, which helps in delocalization of electrons, can be confirmed using fluorescence spectroscopy through a red-shift (shift in spectrum to the right). For example, a yellow fluorescent protein was genetically mutated by replacing Thr203 with Tyr and a red-shifted fluorescence spectrum, i.e., a shift to the right by 0.09eV was observed[37]. From the X-ray structure of the YFP, π-π interaction between the tyrosyl moiety and Tyr203 was observed. Replacing the Tyr203 with other aromatic amino acids resulted in a similar shift[38]. The red-shift can be either due to electrostatic interaction or conformational changes[37]. Therefore, it will be useful to investigate π-stacking for electron delocalization in our genetically mutated curli nanofibers.

2.1.2.2. Effect of pH on Conductive Proteins

In *Geobacter sulfurreducens*, conductivity was found to be highly dependent on pH. The conductivity was higher at low pH and decreased as the pH increased. At pH 2, 7 and 10.5; the conductivity was found to be 188±34 mS cm^{-1}, 51±19 mS cm^{-1} and 37±15 μS cm^{-1} respectively, for wild-type pili (Figure 2.9)[16]. Moreover, the stacking of the aromatic amino acid in wild-type pili increased at low pH, indicating that aromatic amino acids play a key role in the conductivity of the pili fibers[16]. Lastly, conformational changes were also observed due to the increased π-π stacking at lower pH[16]. The increased π-π stacking at lower pH was hypothesized from an X-ray diffraction study. A 100-fold increase in intensity was observed for a peak signifying 3.2 Å spacing at pH 2, thereby resulting in a 100-fold increase in conductivity at pH 2.

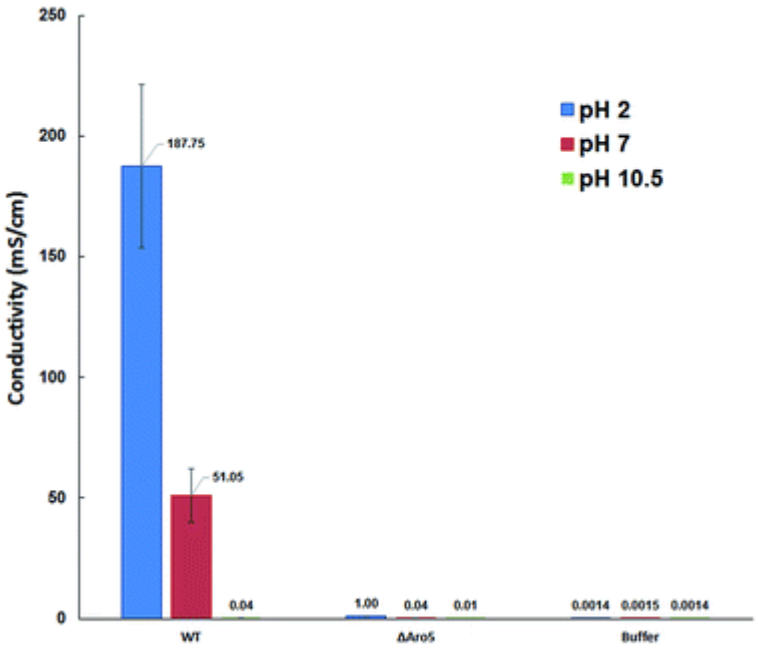

Figure 2.9. Comparison of conductivities of WT pili with mutated pili lacking aromatic residues (tyrosine and phenylalanine) at different pH[16].

2.1.2.3. Effect of Humidity on Conductive Proteins

Humidity can influence the conductivity mechanisms of proteins[7,39]. Depending on the relative humidity (RH), the contribution of protons in the conductivity of proteins can vary[40]. Moreover, the hydration level can affect the morphology of the protein to enable ionic conductivity.

Studies performed by Ashkenasy *et al*. showed increased conductivity of nanotube films in which two phenylalanine residues were replaced by two non-natural 2-thienylalanine (2-Thi) amino acids, resulting in conductance in the range of pS at low-pressure[41,42]. Further research showed that this low conductance could be increased by increasing the relative humidity, therefore,

indicating a role of proton in the high conductivity at high relative humidity (RH). From these studies, it was concluded that below 60% RH, conduction was due to both electrons and protons in the ratio 1:2 respectively[40]. However, at high RH, conduction was only due to protons and in the order of nS.

Another research performed to study the humidity effect on the electrical conductivity of curli mutant protein hydrogels, showed that humidity played a key role in maintaining the conductance of the curli mutant films. Samples which were kept in a humid environment either maintained or showed an increase in their conductance after several days. Several curli mutants were tested and it was observed that Trp1 mutant showed the highest conductance for one row mutation[7]. However, it was not clear which conductivity mechanisms apply for curli fibers from these results.

2.1.2.4. Effect of Temperature on Conductive Proteins

Another factor that effects conductivity in proteins is temperature. Different temperature-conductivity trends were observed depending on the environment of the protein. Conductivity behaviors like semiconductor (increase in conductivity with increase in temperature) or metallic-like conduction (decrease in conductivity with increase in temperature) have been observed in proteins. In semiconductors, with the increase in temperature more electrons become available for conduction and therefore, conductivity increases. However, since there are a lot of free electrons in metals, the increase in temperature results in molecular vibration which impedes the flow of electrons, thereby, resulting in low conductivity.

The effect of temperature on conductivity was observed on *Geobacter sulfurreducens* and was found that conductivity increased with decreasing temperature, indicating non-hopping

conductivity mechanism[11,17]. Reguera *et al.* observed an opposite trend for single fiber measurement at room temperature, which can likely be due to hopping mechanism. Soft materials like biologicals can have different conduction mechanisms based on the level of aggregation [43].

Malvankar *et al.* observed that above 260 K, the inflection point, there was an exponential increase in conductivity upon cooling and below 260 K, there was an exponential decrease in conductivity upon heating (Figure 2.10 a)[11]. Temperature relationship of this type was observed in organic metals, and it was concluded to be due to trap localization below the transition temperature in metallic-like band transport and reduced phonon scattering above it[44].

Hochbaum *et al.* observed that purified pili fibers in aqueous solution had a low exponential temperature dependence above and below the room temperature (Figure 2.10 b)[45]. The low dependence might be due to the thermally-induced conformational changes observed in the protein fibers. It was also suggested to have a possibility of frequency resonance (FR) mechanism, as the probability of coupling between the electronic states can be reduced by thermal disorder. Since measurements performed by the three groups were under different environmental conditions, different conduction mechanisms are possible.

Temperature dependence for another self-assembling antiparallel coiled coil-hexamer peptide (ACC-Hex nanofiber) was studied. The peptide was lacking π-stacking, extended conjugation or redox centers. It was observed that the conductance increases with decreasing temperature, i.e., as the temperature decreases, the electron flow increases resulting in higher conductivity. Therefore, the peptide was found to exhibit metallic like conduction (Figure 2.10 c)[46].

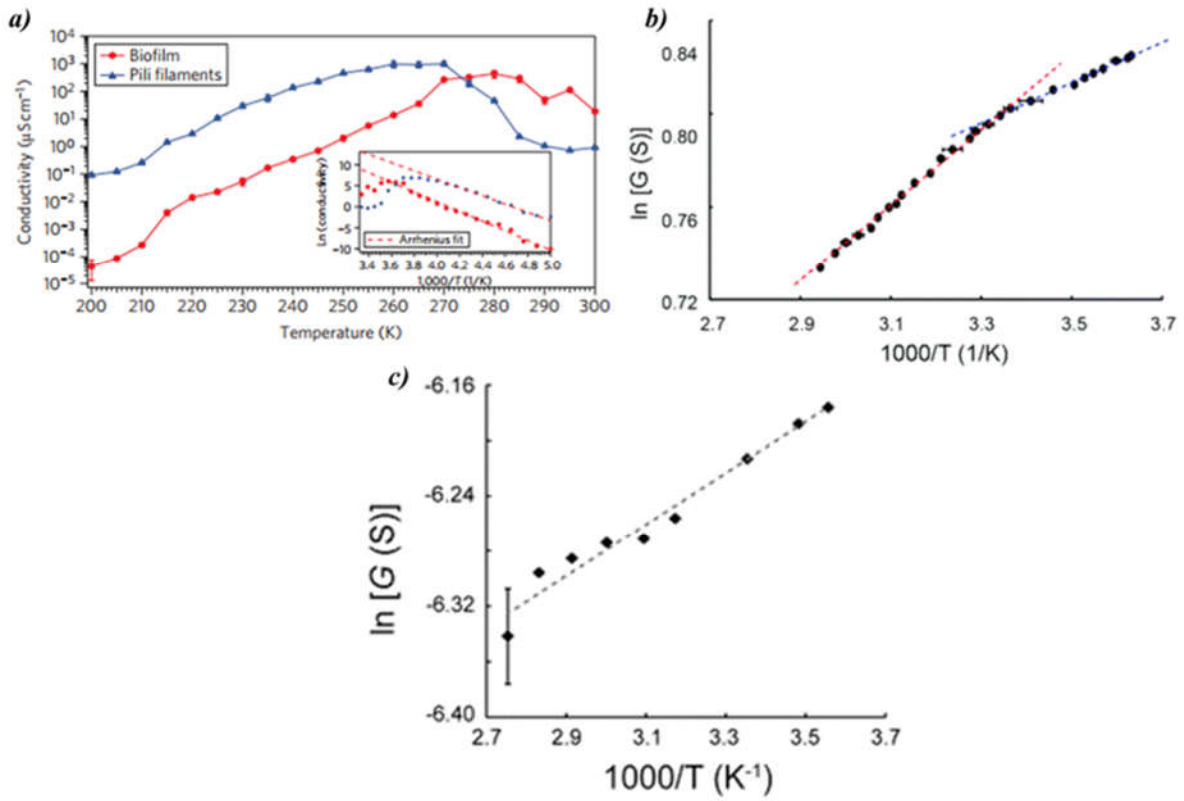

Figure 2.10. a) Temperature dependence of the conductivity of free-standing biofilm formed by *G. sulfurreducens* strain CL-1 and pili filaments of strain KN400 measured with a four-probe method[17], b) Conductivity characteristics of temperature dependence for a film of *G. sulfurreducens* pili nanofibers performed in aqueous environment[45], c) Temperature dependence of ACC-Hex nanofiber peptide at 10 different V_{DS} offsets[46].

2.2. Self-healing in Proteins

Self-healing is a property that allows materials to restore their properties after scratch or damage, either by itself or by the use of an external agent such as heat, pressure, water, etc. Conductive hydrogels, which possess both electrical conductivity and hydrogel softness, have gained attention for their fabrication in biosensors, wearable devices and artificial skin for soft robotics[47]. Hydrogels were made conductive by adding conductive fillers like carbon nanotubes[48], graphene[49], and metallic particles[50] into the polymer. However, there is a drawback to this technique as it results in aggregation of the conductive particles, thereby resulting in low

conductivity or mechanical properties. Another approach for producing conductive hydrogel is by *in situ* polymerization of conjugated precursors for generating conducting polymers like polyaniline (PANI), polypyrrole and polythiophene in the hydrogel[51]. These conductive hydrogels have high electrical conductivity and mechanical properties; however, the brittle network of polymers restricts their applications. Moreover, these polymers are synthesized from non-renewable resources making them non-sustainable for the environment.

A sustainable solution would be proteins which can self-heal. Self-healing proteins can be found in nature such as marine barnacles[52,53]. Studies are being performed to copy the interfacial chemistry of marine barnacles[53]. The characteristics in proteins of our interest would be both conductivity and self-healing ability. As mentioned before, curli nanofibers were genetically engineered to make them electrically conductive. Testing the self-healing property for the engineered curli films is useful in developing stretchable, healable, and environmentally friendly wearable sensors.

2.3. Thesis Summary and Objectives

The overall objective of this thesis is to characterize the genetically engineered proteins, structurally and electrically, to gain better understanding of the conductivity mechanisms. The proteins have been engineered to become conductive by incorporating aromatic amino acid residues. These residues are double-bond ring structures which can help in electron delocalization via π-stacking. In order to confirm π-stacking, and the secondary structure of the protein, fluorescence, Raman spectroscopy and circular dichroism were performed. Furthermore, in order to make flexible, stretchable and healable bio-electronic materials, the self-healing ability was tested. Electrical characterization of the curli films can help us gain knowledge about how

conductivity changes with different environmental parameters and see if we can understand conductivity mechanism of the protein films. Lastly, self-healing tests were performed to determine if we can use them as self-healable sensors. Therefore, the specific objectives of this thesis are listed below and illustrated in Figure 2.11:

- ✓ To understand the interaction between aromatic amino acids by performing structural characterization on the Trp1 mutant protein fibers, thereby studying conductivity mechanism and conformation (folding and aggregation) under different environmental conditions;
- ✓ To gain insight into the conductivity mechanism of curli films by conducting electrical characterization to see the effect of varying pH, thickness and drying with time;
- ✓ To study electrical healing of Trp1 mutant films, electrical characterization of scratch and rehydrated films was performed.

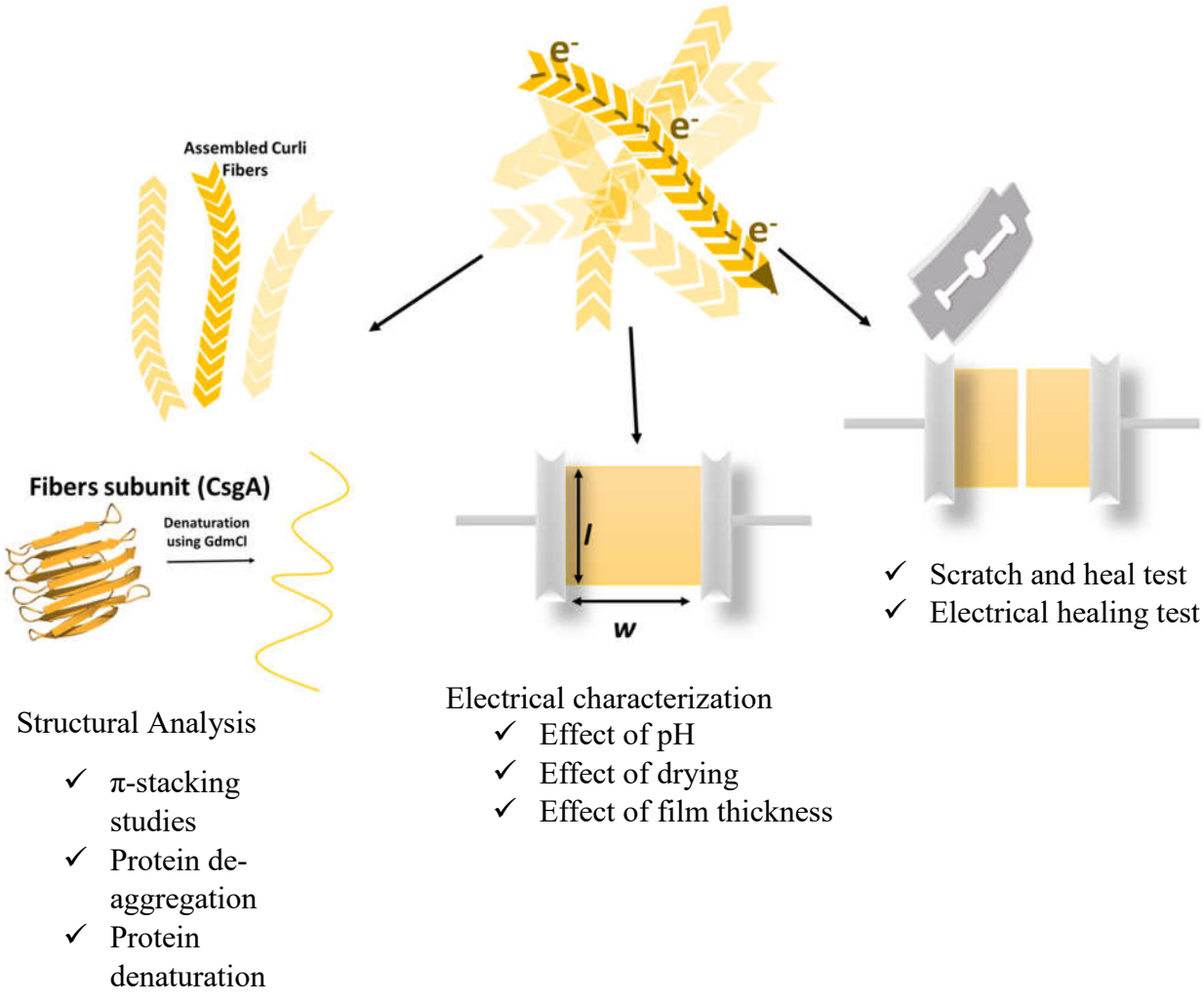

Figure 2.11. Schematic representation of the objectives, left panel: structural analysis of curli fibers, middle panel: electrical characterization of the mutant proteins, right panel: self-healing test on curli films.

2.4. References

1. Gutowski, T. G. *et al.* Thermodynamic Analysis of Resources Used in Manufacturing Processes. *Environ. Sci. Technol.* **43,** 1584–1590 (2009).
2. Irimia-Vladu, M. "Green" electronics: biodegradable and biocompatible materials and devices for sustainable future. *Chem. Soc. Rev.* **43,** 588–610 (2014).
3. Roychoudhuri, R. *et al.* Estimation of E-waste Generation—A Lifecycle-Based Approach. in *Waste Management and Resource Efficiency* 825–832 (Springer Singapore, 2019). doi:10.1007/978-981-10-7290-1_69
4. *THE GLOBAL E-WASTE MONITOR 2014 Quantities, flows and resources*.
5. Alfinito, E., Reggiani, L. & Pousset, J. Proteotronics: Electronic devices based on proteins. in *Lecture Notes in Electrical Engineering* **319,** 3–7 (Springer Verlag, 2015).
6. Alfinito, E., Pousset, J. & Reggiani, L. *Proteotronics: Development of protein-based electronics*. *Proteotronics: Development of Protein-Based Electronics* (Pan Stanford Publishing Pte. Ltd., 2015). doi:10.1201/b18966
7. Dorval Courchesne, N.-M. *et al.* Biomimetic engineering of conductive curli protein films. *Nanotechnology* **29,** 454002 (2018).
8. Amdursky, N. Enhanced solid-state electron transport via tryptophan containing peptide networks. *Phys. Chem. Chem. Phys.* **15,** 13479 (2013).
9. Ashkenasy, N., Horne, W. S. & Ghadiri, M. R. Design of self-assembling peptide nanotubes with delocalized electronic states. *Small* **2,** 99–102 (2006).
10. Walker, D. J. F. *et al.* The Archaellum of Methanospirillum hungatei Is Electrically Conductive. (2019). doi:10.1038/nmicrobiol.2016.222
11. Malvankar, N. S. *et al.* Structural basis for metallic-like conductivity in microbial nanowires. *MBio* **6,** e00084 (2015).
12. Reardon, P. N. & Mueller, K. T. Structure of the type IVa major pilin from the electrically conductive bacterial nanowires of Geobacter sulfurreducens. *J. Biol. Chem.* **288,** 29260–6 (2013).
13. Reguera, G., Nevin, K., … J. N.-A. and & 2006, undefined. Biofilm and nanowire production leads to increased current in Geobacter sulfurreducens fuel cells. *Am Soc Microbiol*
14. Reardon, P., Chemistry, K. M.-J. of B. & 2013, undefined. Structure of the type IVa major pilin from the electrically conductive bacterial nanowires of Geobacter sulfurreducens. *ASBMB*
15. Tan, Y. *et al.* Synthetic Biological Protein Nanowires with High Conductivity. *Small* **12,** 4481–4485 (2016).
16. Adhikari, R. Y., Malvankar, N. S., Tuominen, M. T. & Lovley, D. R. Conductivity of

individual Geobacter pili. *RSC Adv.* **6,** 8354–8357 (2016).

17. Malvankar, N. S. *et al.* Tunable metallic-like conductivity in microbial nanowire networks. *Nat. Nanotechnol.* **6,** 573–579 (2011).

18. Vargas, M. *et al.* Aromatic amino acids required for pili conductivity and long-range extracellular electron transport in Geobacter sulfurreducens. *MBio* **4,** e00105-13 (2013).

19. Malvankar, N. S. *et al.* Structural basis for metallic-like conductivity in microbial nanowires. *MBio* **6,** e00084 (2015).

20. Liu, L. *et al.* Electrochemical fabrication and electronic behavior of polypyrrole nano-fiber array devices. *Thin Solid Films* **503,** 241–245 (2006).

21. Tans, S. J. *et al.* Individual single-wall carbon nanotubes as quantum wires. *Nature* **386,** 474–477 (1997).

22. Barnhart, M. M. & Chapman, M. R. Curli Biogenesis and Function. *Annu. Rev. Microbiol.* **60,** 131–147 (2006).

23. Dorval Courchesne, N.-M., Duraj-Thatte, A., Tay, P. K. R., Nguyen, P. Q. & Joshi, N. S. Scalable Production of Genetically Engineered Nanofibrous Macroscopic Materials via Filtration. *ACS Biomater. Sci. Eng.* **3,** 733–741 (2017).

24. Sitaras, C., Naghavi, M. & Herrington, M. B. Sodium dodecyl sulfate–agarose gel electrophoresis for the detection and isolation of amyloid curli fibers. *Anal. Biochem.* **408,** 328–331 (2011).

25. Goyal, P. *et al.* Structural and mechanistic insights into the bacterial amyloid secretion channel CsgG. *Nature* **516,** 250–253 (2014).

26. Zhou, Y., Smith, D. R., Hufnagel, D. A. & Chapman, M. R. Experimental Manipulation of the Microbial Functional Amyloid Called Curli. in 53–75 (Humana Press, Totowa, NJ, 2013). doi:10.1007/978-1-62703-245-2_4

27. Collinson, S. K., Emödy, L., Müller, K. H., Trust, T. J. & Kay, W. W. Purification and characterization of thin, aggregative fimbriae from Salmonella enteritidis. *J. Bacteriol.* **173,** 4773–81 (1991).

28. Chapman, M. R. *et al.* Role of Escherichia coli Curli Operons in Directing Amyloid Fiber Formation. *Science (80-.).* **295,** 851–855 (2002).

29. Tao, K., Makam, P., Aizen, R. & Gazit, E. Self-assembling peptide semiconductors. *Science* **358,** eaam9756 (2017).

30. LADIK, J. Energy Band Structure of Proteins. *Nature* **202,** 1208–1209 (1964).

31. Evans, M. G. & Gergely, J. A discussion of the possibility of bands of energy levels in proteins electronic interaction in non bonded systems. *Biochim. Biophys. Acta* **3,** 188–197 (1949).

32. Horowitz, G., Hajlaoui, M. E. & Hajlaoui, R. Temperature and gate voltage dependence of hole mobility in polycrystalline oligothiophene thin film transistors. *J. Appl. Phys.* **87,**

4456–4463 (2000).

33. Orton, J. W. & Powell, M. J. The Hall effect in polycrystalline and powdered semiconductors. *Reports Prog. Phys.* **43,** 1263–1307 (1980).

34. Lakowicz, J. R. *Principles of Fluorescence Spectroscopy Third Edition*. (2006).

35. Permyakov, E. A. Luminescent Spectroscopy of Proteins - Eugene A. Permyakov - Google Books. Available at: https://books.google.ca/books?id=NrxHDwAAQBAJ&pg=PT46&lpg=PT46&dq=Burstein+EA,+1976.+luminescence+of+protein+chromophores.+In+model+studies,+science+and+technology+results&source=bl&ots=qrW5ZQqQug&sig=ACfU3U2sp5lPiJFpWwELPFyVMYKVzGMowQ&hl=en&sa=X&ved=2ahU. (Accessed: 9th June 2019)

36. Vivian, J. T. & Callis, P. R. Mechanisms of Tryptophan Fluorescence Shifts in Proteins. *Biophys. J.* **80,** 2093–2109 (2001).

37. Park, J. W. & Rhee, Y. M. Emission shaping in fluorescent proteins: Role of electrostatics and π-stacking. *Phys. Chem. Chem. Phys.* **18,** 3944–3955 (2016).

38. Kummer, A. D. *et al.* Effects of Threonine 203 Replacements on Excited-State Dynamics and Fluorescence Properties of the Green Fluorescent Protein (GFP). *J. Phys. Chem. B* **104,** 4791–4798 (2000).

39. Yamahata, C. *et al.* Humidity Dependence of Charge Transport through DNA Revealed by Silicon-Based Nanotweezers Manipulation. *Biophys. J.* **94,** 63–70 (2008).

40. Amit, M. *et al.* Hybrid Proton and Electron Transport in Peptide Fibrils. *Adv. Funct. Mater.* **24,** 5873–5880 (2014).

41. Amit, M., Cheng, G., Hamley, I. W. & Ashkenasy, N. Conductance of amyloid β based peptide filaments: structure–function relations. *Soft Matter* **8,** 8690 (2012).

42. Giese, B. *et al.* Electron Relay Race in Peptides. *J. Org. Chem.* **74,** 3621–3625 (2009).

43. Lampa-Pastirk, S. *et al.* Thermally activated charge transport in microbial protein nanowires. *Sci. Rep.* **6,** 23517 (2016).

44. Kaiser, A. B. Systematic Conductivity Behavior in Conducting Polymers: Effects of Heterogeneous Disorder. *Adv. Mater.* **13,** 927–941 (2001).

45. Ing, N. L., Nusca, T. D. & Hochbaum, A. I. Geobacter sulfurreducens pili support ohmic electronic conduction in aqueous solution. *Phys. Chem. Chem. Phys.* **19,** 21791–21799 (2017).

46. Ing, N. L., Spencer, R. K., Luong, S. H., Nguyen, H. D. & Hochbaum, A. I. Electronic Conductivity in Biomimetic α-Helical Peptide Nanofibers and Gels Article. *ACS Nano* **12,** (2018).

47. Guiseppi-Elie, A. Electroconductive hydrogels: Synthesis, characterization and biomedical applications. *Biomaterials* **31,** 2701–2716 (2010).

48. Cai, G. *et al.* Extremely Stretchable Strain Sensors Based on Conductive Self-Healing

Dynamic Cross-Links Hydrogels for Human-Motion Detection. *Adv. Sci.* **4,** 1600190 (2017).

49. Jing, X., Mi, H. Y., Peng, X. F. & Turng, L. S. Biocompatible, self-healing, highly stretchable polyacrylic acid/reduced graphene oxide nanocomposite hydrogel sensors via mussel-inspired chemistry. *Carbon N. Y.* **136,** 63–72 (2018).

50. You, J.-O. & Auguste, D. T. Conductive, Physiologically Responsive Hydrogels. *Langmuir* **26,** 4607–4612 (2010).

51. Balint, R., Cassidy, N. J. & Cartmell, S. H. Conductive polymers: Towards a smart biomaterial for tissue engineering. *Acta Biomaterialia* **10,** 2341–2353 (2014).

52. Holten-Andersen, N., Fantner, G. E., Hohlbauch, S., Waite, J. H. & Zok, F. W. Protective coatings on extensible biofibres. *Nat. Mater.* **6,** 669–672 (2007).

53. Lee, B. P., Messersmith, P. B., Israelachvili, J. N. & Waite, J. H. Mussel-Inspired Adhesives and Coatings. *Annu. Rev. Mater. Res.* **41,** 99–132 (2011).

Chapter 3 : Structural and Spectroscopic Characterization of Conductive Tryptophan-Containing Curli Fibers

In this chapter, we performed spectroscopic studies for analyzing tryptophan-containing curli fibers to better understand their conductivity mechanism. Information obtained from the spectroscopic analysis in this chapter will be helpful in correlating the conductivity mechanism with the results proposed in chapter 3 based on electrical characterization.

3.1. Introduction

Charge transport in conductive mutants curli nanofibers may be useful in several applications including biosensors, environmental-stimuli sensors, or in microbial fuel cells to generate electric current. Therefore, it is important to understand the charge-transport mechanism along these protein nanofibers. Biological proteins are generally non-conductive[1–3]; however, our mutant curli nanofibers (Trp1, Tyr1, Phe1) represent a genetically engineered class of electronically functional proteins, which can be used in bioelectronic applications. Conductive curli nanofibers could serve as an alternative for synthetic conductive polymers, as they are biodegradable, non-toxic, economical and can be easily scaled up using bacteria as green material factories[4].

An intensively studied naturally conductive protein pili secreted from *Geobacter* contains aromatic amino acids. The self-assembling pili of *Geobacter sulfurreducens* exhibit long-range electron transfer[5]. These proteins are analogous to the mutant curli nanofibers because of their high density of aromatic residues. However, pili proteins are not scalable, unlike curli nanofibers which have previously been scaled up via a vacuum filtration protocol[4]. Previous studies on *G. sulfurreducens* pili concluded that charges could be transported over micrometer distances along

the length of pili fiber. To investigate the conductivity mechanism in pili fibers, selected aromatic amino acids have been replaced with alanine (non-aromatic amino acid), thereby decreasing conductivity. This decrease in conductivity shows that aromatic amino acids in the pili structure had a key role to play in electron transport over long distances. Moreover, a pH-dependence study performed on *Geobacter* pili showed a 100-fold increase in conductivity with a decrease in pH from 10.5 to 2, due to electron delocalization via π-π stacking of the aromatic rings[6,7]. Taking inspiration from pili of *Geobacter sulfurreducens,* curli fibers were genetically engineered with aromatic amino acids to make the fibers conductive[8].

Previously, modeling studies have been performed to characterize the CsgA structure (the main subunit of curli fibers)[8,9], however, no experimental data is available to confirm its structure. It is, therefore, important to perform structural characterization on the conductive mutant curli nanofibers to understand the effect of solvents and environmental conditions (such as pH aggregation and unfolding of proteins) on the structure of the proteins. Characterizing the conformation of the CsgA subunits will give us insights about the local environment of the aromatic residues within the proteins, and their positions relative to each other which will in turn help us understand the conductivity mechanism for charge transport.

Fluorescence spectroscopy is a useful technique for characterizing proteins with aromatic amino acids. The presence of aromatic amino acids can easily be detected using fluorescence spectroscopy, since the proteins have been mutated with tryptophan residues for the following mutants, Trp1 and random Trp. Trp1 mutant has one row tryptophan residues bridging over the five repeats of their β-sheet structure[8] and random Trp has tryptophan residues randomly positioned. From Table 3.1, since tryptophan is the dominant fluorophore amongst the three aromatic amino acids, it will be useful to use Trp1 mutant over Tyr1 mutant and Phe1 mutant[10],

and use random Trp mutant as a control. Using these proteins for spectroscopic measurements will help us understand the conductivity mechanism based on the protein conformation. Therefore, observing the conformational change in the form of an emission peak shift to the right will help us gain insight into the π-stacking of the aromatic rings responsible for electron delocalization.

Table 3.1. Excitation and emission wavelengths of the aromatic amino acids

Fluorophore	Excitation Wavelength (nm)	Emission Wavelength (nm)
Tryptophan	295	348
Tyrosine	275	303
Phenylalanine	240	282

Second, circular dichroism (CD), a technique to study the secondary structure of proteins, can be used to experimentally to confirm the secondary structure of the CsgA mutants by measuring the difference in absorbance of right and left-circularly polarized light by the curli fibers. Bands at different positions are observed for different secondary structures. A α-helical protein has two negative bands around 222 and 208 nm and a positive band at 190 nm. A β-sheet protein has a negative band between 210-220 nm and a positive band between 195-200 nm[10].

3.2. Materials & Methods

3.2.1. Curli Nanofibers Expression and Purification

Plasmids coding for mutant curli fibers were transformed in an *E. coli* strain, PQN4, from which all the curli specific genes (*csgBAC* and *csgDEFG*) were deleted[4]. They were then streaked on lysogeny broth (LB) agar plates which were incubated at 37º C overnight. A small-scale culture was prepared by picking a colony and inoculating in 5 ml LB medium, 100 µg/mL carbenicillin

and 2% (m/v) glucose to suppress the expression of curli fiber proteins in the small-scale culture. The culture was grown for overnight at 37 ºC and 325 rpm, followed by a large-scale culture by diluting the small-scale culture in 1:100 LB medium with 100 µg/mL carbenicillin for 24 hours at 37 ºC and 325 rpm.

Purification of the proteins was performed by an established vacuum filtration protocol[4]. Briefly, the large-scale culture was incubated for an hour in 0.8 M GdmCl before filtration. The culture was then filtered onto a 10 µm polycarbonate membrane, followed by incubating for 5 minutes in 8 M GdmCl for cell lysis remaining in the culture and to denature the proteins other than curli nanofibers. It was rinsed thoroughly with deionized (DI) water, followed by incubating in benzonase nuclease for 10 minutes to remove nucleic acids. This step was performed to degrade nucleic acids and was followed by another rinsing step. To delaminate the protein from the filter membrane, sodium dodecyl sulfate (SDS) at a concentration of 5% (m/v) was incubated for 5 minutes and was thoroughly rinsed out. The resulting protein hydrogels were scraped off from the filter membrane using a spatula and stored at 4 ºC.

3.2.2. Confirmation of Expression of Mutant Proteins

The expression of curli protein nanofibers was confirmed by performing a Congo Red assay on 1 mL bacterial culture suspension right before filtration[4]. The culture was first centrifuged for 10 minutes at 10,000 rpm and then the supernatant was discarded leaving behind a pellet which was resuspended in phosphate buffer. Then, 100 µL of 0.001 M Congo Red dye was added to the buffer suspension and incubated for 10 minutes, and then centrifuged 10 minutes at 10,000 rpm. To quantify the amount of Congo Red that did not bind to the amyloid fibers, the absorption of the supernatant at 490 nm was measured. There were two controls for this experiment, bacteria

expressing WT fibers as the positive control, and bacteria expressing a soluble maltose binding protein (MBP) as the negative control.

3.2.3. SDS-PAGE

SDS-PAGE was used to assess the purity of the filtered samples. WT, Trp1 and His1 proteins containing his-tag were used for the test. Lyophilized samples were disassembled using 1:1 (v/v) HFIP/TFA mixture. The mixture was sonicated until the solution appeared clear and the solvent was then evaporated. DI water and loading buffer were then added to the samples. SDS-PAGE gel was run using Bio-Rad electrophoresis chamber.

3.2.4. Scanning Electron Microscopy (SEM)

Samples were prepared by filtering bacterial cultures on a 10 μm pore size polycarbonate filter membrane to image proteins secreted by the bacteria. These samples were washed with 0.1 M sodium cacodylate buffer and then fixed with 2% glutaraldehyde and 2% paraformaldehyde. The samples were then washed in water bath followed by ethanol baths for 15 minutes with gradually increasing concentration of ethanol (25%, 50 %, 75 %, 100% (v/v)). Samples were then dried using Leica Microsystems EM CPD030 Critical Point Dryer and a Leica Microsystems EM ACE600 High Resolution Sputter Coater with a 5 nm layer of Pt. SEM imaging was performed using FEI Inspect F50 FE-SEM.

3.2.5. Circular Dichroism

Circular Dichroism (CD) was performed to confirm the secondary structure of the proteins. 0.5 mg of the lyophilised fibers were suspended in 1 mL water and incubated with sonication for 10 minutes. Triplicate readings were performed on a single sample of 200 μL and the average data

was plotted. CD measurements were performed using quartz cuvette in a Chirascan instrument and the data was analysed using Chirascan software.

3.2.6. Raman Spectroscopy

Raman spectroscopy was used to confirm the presence of Trp residues in the Trp1 mutant. Filtered hydrogel was drop-casted onto a glass slide and dried in ambient air. Measurements were performed on five separate locations and the readings were averaged and plotted. The measurements were performed using an Alpha300R Raman Spectrometer and the image was processed using the software Project 5 Plus.

3.2.7. Fluorescence Spectroscopy

All the fluorescence measurements were performed using an infinitPro plate reader using a Corning 96-well Flat Bottom Black Polystyrol plate at room temperature, with an emission wavelength in the range of 300-400 nm, and step size of 1 nm. Error bars were plotted to represent the standard deviation between the measurements.

To study the conformation of the four protein samples, Trp1 mutant, His1 mutant, Trp random mutant and WT, 0.5 mg of lyophilized fibers were suspended in 1 mL of DI water to obtain a concentration of 0.5 mg/mL. They were excited at a wavelength of 290 nm. Triplicate measurements were taken and averaged. Water (as the blank sample) emission were used as the baseline and were subtracted from the averaged data prior to plotting.

To study the effect of pH on the Trp1 mutant, an emission scan in the range of 300-400 nm with 290 nm excitation wavelength and an excitation scan in the range of 250-350 nm with 326 nm emission wavelength were performed. The Trp1 mutant was prepared by suspending 0.5 mg of lyophilized fibers in 1 mL of Carmody buffer at pH 10.5 to obtain a concentration of 0.5

mg/mL. The Carmody buffer was prepared by mixing 49 mL of solution A (0.2 M boric acid and 0.05 M citric acid) and 151 mL of solution B (0.1 M Tertiary Sodium Phosphate). Triplicate measurements were taken and averaged; the buffer was then titrated with a total of 10 µL 1 M HCl to reach pH 7. Triplicate measurements were performed again and averaged. The buffer was titrated for the second time by adding 15 µL of 1 M HCl to reach down to pH 2, and triplicate measurements were taken. Respective pH buffer baselines were subtracted from the averaged data prior to plotting.

To study the effect of GdmCl on protein unfolding, two protein samples were prepared by suspending 0.5 mg of lyophilized Trp1 mutant fibers in 1 mL of DI water and GdmCl respectively to obtain a concentration of 0.5 mg/mL. The samples were excited at three different excitation wavelength, 275 nm, 290 nm, and 295 nm respectively. Triplicate measurements were taken and averaged. Water and GdmCl baselines were subtracted from the averaged data prior to plotting.

3.3. Results & Discussion

3.3.1. Confirmation of Expression of Mutant Proteins

Curli nanofibers were previously genetically mutated with different aromatic amino acids (Trp, Tyr, Phe and His) to render them electrically conductive[8]. We used plasmids containing these mutations along with the WT plasmid and a plasmid encoding for a maltose binding protein (MBP) as controls. These plasmids were transformed in an *E. coli* strain, PQN4, from which all the curli specific genes were deleted from the genome[4]. By deleting these curli genes from the genome of PQN4, the curli nanofibers expressed will be as a result of the "synthetic operon" (*csgBACEFG*) present in the mutated plasmid, and there will be no genomic expression of natural curli fibers.

Expression of the curli nanofibers (WT and with mutations) was performed using a scalable vacuum filtration protocol using guanidine hydrochloride as denaturing agent to reduce the number and concentration of impurities, DNase to degrade nucleic acids (DNAs and RNAs), and SDS to facilitate the delamination of the purified protein hydrogel from the filter membrane by using a spatula.

To assess the expression of curli nanofibers, Congo Red dye binding assay and scanning electron microscope (SEM) was used. Congo Red is a dye which binds specifically to amyloid fibers. Since curli proteins have an amyloid fold, the dye should bind to the fibers expressed by the PQN4 cells. It was observed that irrespective of the aromatic mutations, curli nanofibers were expressed by the PQN4 and formed amyloid fibers, as seen from Figure 3.1(a-b). A quantitative analysis of the Congo Red dye that remained unbound in the supernatant showed that the amount of bound dye was slightly higher for the aromatic amino acid mutants compared with WT. This increased dye binding could indicate a higher level of protein expression, or a higher affinity of the Congo Red dye itself for the aromatic mutants, due to either increasing number of hydrophobic residues after mutation resulting in increased aggregation or due to the stabilizing effect of the aromatic rings on the overall structure.

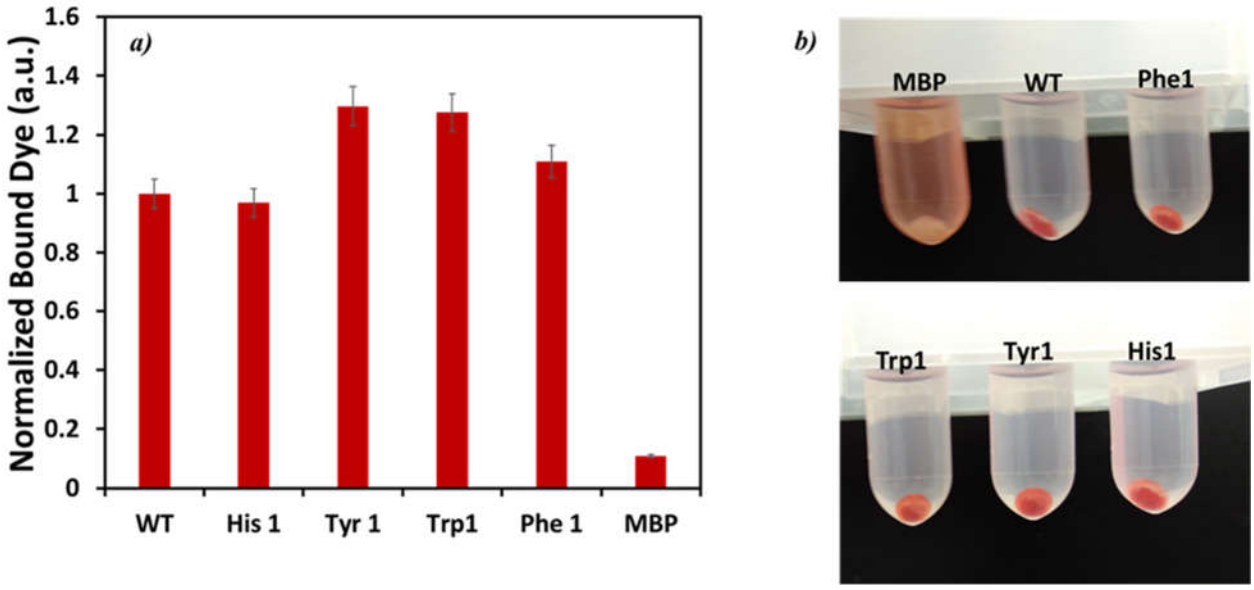

Figure 3.1. Mutant CsgA proteins are successfully expressed by *E. coli*. a) quantitative analysis of amyloid fiber expression using Congo Red assay, b) visual analysis of the Congo Red assay showing successful expression and binding of curli protein mutants to the dye.

SEM images of the expressed curli nanofibers showed that the aromatic amino acid mutant fibers (Trp1 and His1) were expressed and formed fibers with morphology similar to WT fibers. The images show protein fiber aggregates surrounded by *E. coli* bacteria.

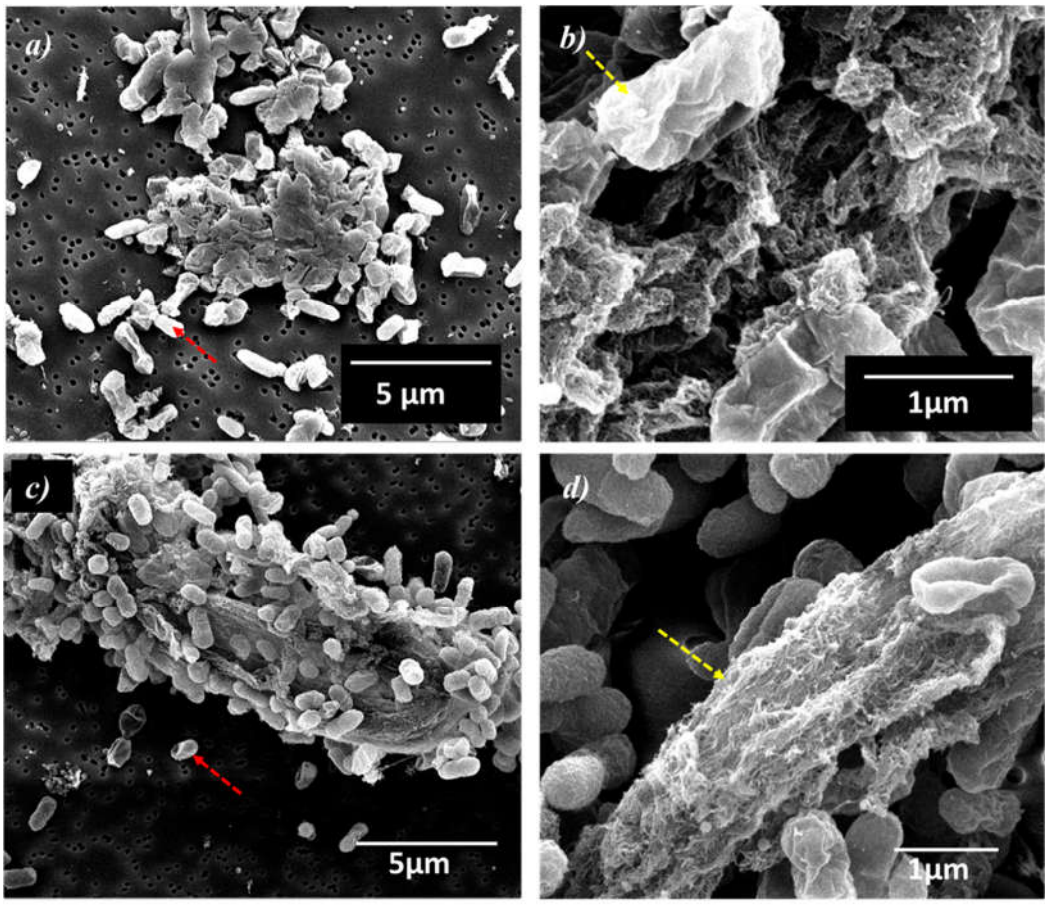

Figure 3.2. Curli fibers self-assemble upon secretion from *E. coli*. SEM images of WT (a-b) and Trp1 (c-d) expressing bacterial cultures, yellow arrows show curli fiber aggregates and red arrows show bacterial cells.

Lastly, the expression of the mutant proteins and secondary structure of the purified proteins were analyzed using SDS-Page and CD, respectively. The expression of the semi-purified mutant proteins containing his-tag were confirmed by running an SDS-Page gel. Trp1 mutant, His1 mutant and WT were around their expected molecular weights, i.e., 14720.33 Da, 16815.01 Da, and 15103.94 Da respectively. From CD, the spectra for the WT and mutant fibers showed bands

indicative of β-sheets: a negative band around 200 to 230 nm and a positive band around 190 nm consistent with the literature was observed.

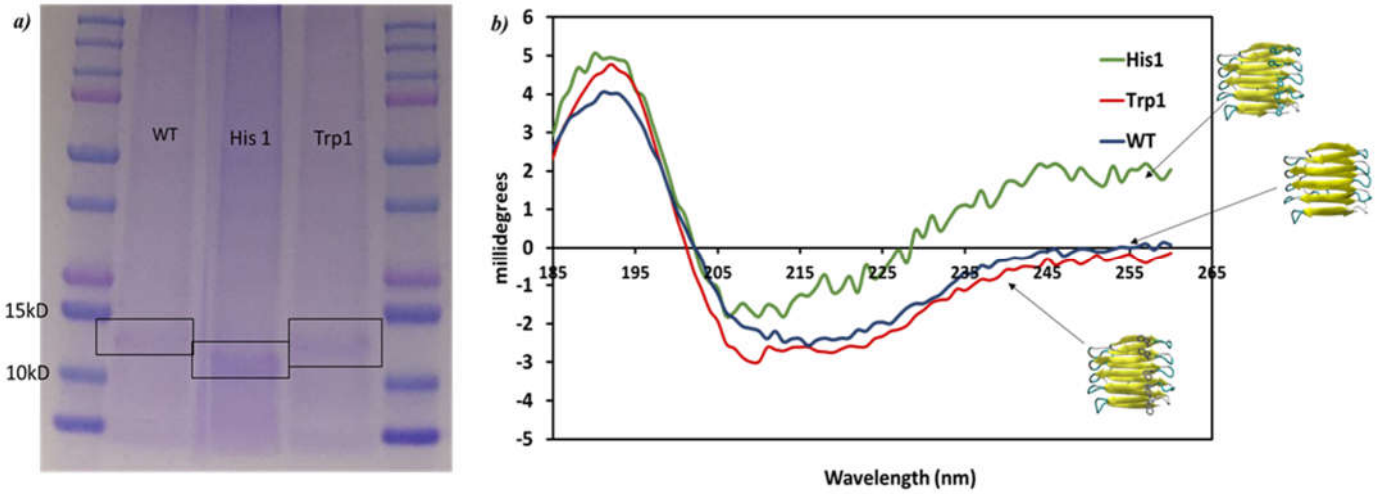

Figure 3.3. Purity and secondary structure study of curli proteins, a) SDS-Page gel confirming the presence of semi-purified CsgA proteins containing his-tag (WT 15103.94 Da, Trp1 14720.33 Da and His1 16815.01 Da) around the expected molecular weights, b) Circular dichroism spectra showing the β-sheet secondary structure of the mutant proteins.

3.3.2. Raman Spectroscopy

The genetic additions of aromatic residues performed on curli fibers can be confirmed using Raman spectroscopy. Different Raman peaks are assigned for different aromatic amino acids (Trp, Tyr, Phe, His). We performed measurements on the Trp1 variant to confirm the presence of Trp residues, which can be observed through higher intensity peaks for tryptophan residues compared to WT or His1 mutant. The higher content of tryptophan residues in Trp1 mutant resulted in evident tryptophan peaks at 759 cm^{-1}, 1208 cm^{-1}, 1555 cm^{-1} and 1618 cm^{-1} (Figure 3.4). The environment of the tryptophan residues can be further investigated from the ratio of the 1360/1340 cm^{-1} peaks. The high ratio between the two peaks suggests hydrophobic environment around the tryptophan residues. Lastly, the expected peak around 1208 cm^{-1} for histidine residues in His1 mutant can not be observed due to the presence of aromatic amino acids.

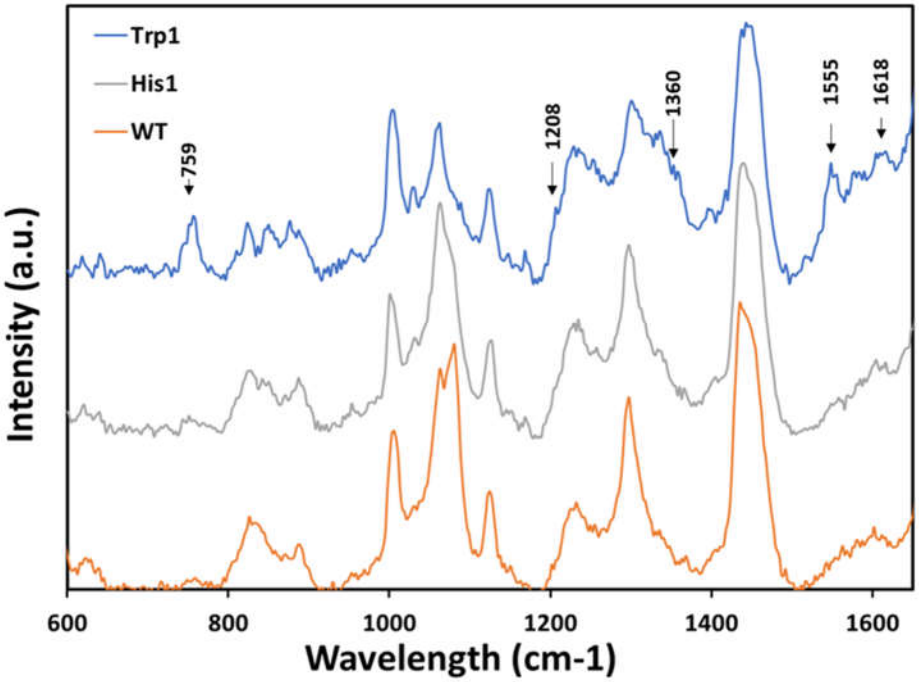

Figure 3.4. Raman Intensity confirming higher content of tryptophan residues in Trp1 mutant compared to His1 mutant and WT.

3.3.3. Analysis of Protein Conformation using Fluorescence Measurements

3.3.3.1. Presence of Tryptophan residues

WT CsgA natively has one tryptophan, two histidine, three phenylalanine and four tyrosine residues. Trp1 and random Trp mutants have a total of six tryptophan, four tyrosine, three phenylalanine and two histidine residues. The His1 mutant has seven histidine, three phenylalanine, four tyrosine, and one tryptophan residues (Table 3.2). The conformational changes due to unfolding/aggregation of CsgA protein containing tryptophan can be observed through the emission spectrum shifts, while the fluorescence intensity can help us gain insight on the protein concentration and the density of aromatic residues per protein. Figure 3.5 shows that the Trp1 mutant exhibits the highest fluorescence intensity compared with the His1 mutant and WT fibers,

for the same mass of proteins. This difference in intensity is a result of the Trp1 mutant being genetically engineered with five extra tryptophan residues, which is the most dominant fluorescent amino acid amongst the three fluorescent amino acids (fluorophores: Trp, Tyr, Phe). The higher fluorescence intensity of the Trp1 mutant is due to the presence of five additional tryptophan residues compared with His1 and WT, which both originally contain only one tryptophan residue.

Table 3.2. Total number of aromatic amino acids in selected single CsgA proteins

Mutant CsgA proteins	Aromatic amino acid residue type			
	Tryptophan	Tyrosine	Phenylalanine	Histidine
WT	1	4	3	2
Trp1	6	4	3	2
His1	1	4	3	7
random Trp	6	4	3	2

From literature, Trp when excited at 290 nm, results in an emission spectrum (maximum wavelength λ_{max}) around 348 nm[10]. However, from Figure 3.5, it can be inferred that the λ_{max} for the three samples are around 330 nm, indicating that the Trp residues are buried away from the solvent in a hydrophobic environment formed by protein aggregation. In fact, a 10-20 nm blue-shift is expected when tryptophan residues are buried in the hydrophobic core of folded proteins[11,12]. Moreover, Trp-Trp resonance energy transfer (RET) can be observed in proteins which display a blue-shifted emission spectrum[10]. This RET is because energy can be easily transferred from one tryptophan emission spectrum to the next tryptophan absorption spectrum located within 4-16 Å, due to the spectral overlap of the absorption spectrum at 280 nm[13] and the blue-shifted Trp1 mutant spectrum at 330 nm. We hypothesize that the energy lost by the first

tryptophan residue is passed on to the next tryptophan residue through RET and therefore, we see an increase in emission intensity for Trp1 mutant.

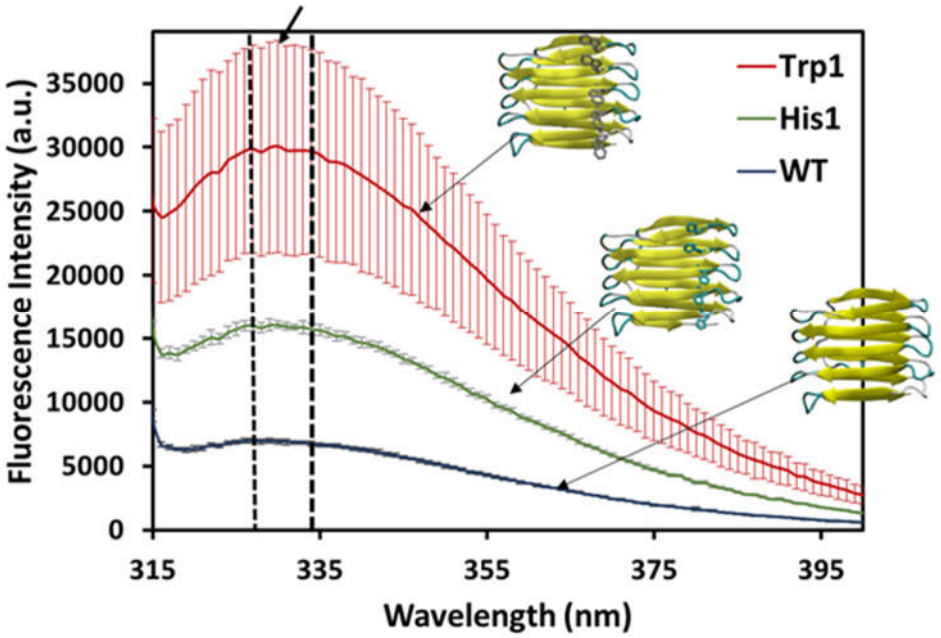

Figure 3.5. The high density of Trp residues in the Trp1 mutant and the hydrophobic environment surrounding the Trp residues can be confirmed from peak intensity and peak position respectively. Emission scan was performed for 0.5 mg/mL Trp1 mutant, His1 mutant and WT when excited at 290 nm over a wavelength of 315-400 nm and 1 nm step size.

3.3.3.2. Investigation of π-stacking between aromatic rings

To gain insights into the mechanism of conductivity through the Trp1 mutant curli nanofibers - i.e., whether conductivity occurs through electron delocalization via π-π stacking of aromatic residues, or due to electron hopping through the backbone structure - emission scans for the Trp1 mutant and the random Trp mutant were performed. Studying the spectrum of these two mutants can help us understand whether the Trp residues (aligned in one row in Trp1) are π-stacking, since the same number of Trp residues are found in both mutants, but the positioning of the residues varies. In Trp1, the residues in close proximity to each other, while in random Trp,

the residues are far from each other, dispersed randomly on the exterior surface of CsgA (Figure 3.6 a-c) . A distance between the aromatic rings of 5 Å or less is necessary for electron delocalization via π-orbitals[8]. The distance between the aromatic rings in Trp1 mutant was

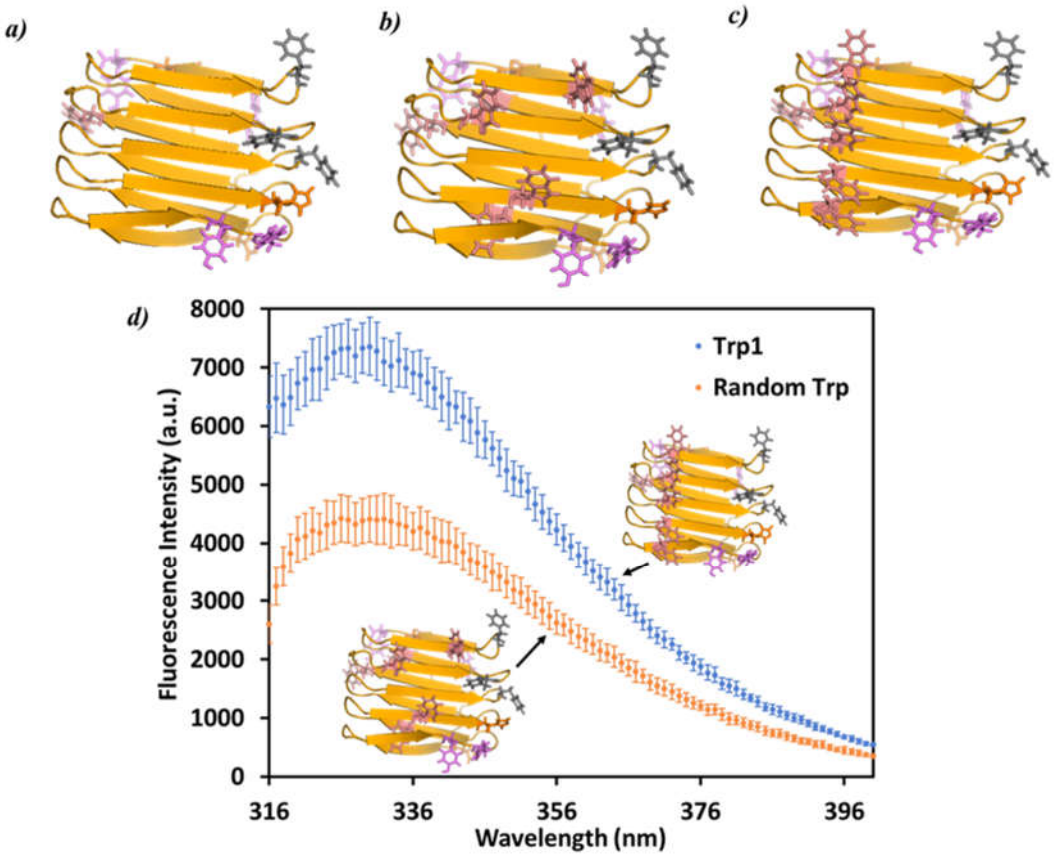

Figure 3.6. Red-shift for Trp1 mutant suggests π-stacking between the rings. a) through c) Pymol images of CsgA monomer showing all of the aromatic amino acids presents in WT and mutant CsgA proteins. Salmon (tryptophan), grey (phenylalanine), violet (tyrosine), orange (histidine) in a) WT, b) random Trp mutant, c) Trp1 mutant. d) Trp1 mutant fluorescence peak is shifted to the right indicated by an arrow and random Trp mutant peak is shifted to the left also indicated by an arrow.

measured using Pymol and was found to be 3.16 Å for the closest and 5.55 Å for the farthest adjacent rings. We observed that the Trp1 mutant had its emission peak at 330 nm while the random Trp mutant was blue-shifted and had its peak at 326 nm (Figure 3.6 d). This observation

indicates that the Trp1 mutant is red-shifted which hints towards possibility of π-π stacking between the aromatic rings for the delocalization of electrons.

3.3.4. Effect of Environment

3.3.4.1. Change in pH on Trp1 mutant

To study the effect of environmental stimuli, like pH, on the Trp1 mutant, emission and excitation scans were performed by varying the pH of the Trp1 mutant media (Figure 3.7 a-b). Understanding the conformational changes at different pHs could help correlate the effect of different pHs on protein folding and aggregation, and how these correlated with the conductivity of Trp1 mutant. As mentioned previously, in order to excite tryptophan residues, the emission scan was performed at 295 nm. We observed that at pH 2, the emission peak was located at 325 nm, about 3 nm to the left compared to the emission spectrum of pH 7 which was around 329 nm, while pH 10 had the emission peak around 334 nm which was red-shifted (Figure 3.7 a). This gradual spectral shift to the right with increasing pH from pH 2 to pH 10, indicates that the tryptophan residues are exposed to the solvent, i.e., the residues are exposed to a more hydrophilic environment at pH 10. However, at pH 2 Trp residues are buried in a more hydrophobic environment, due to protein aggregation, away from the solvent. Moreover, the emission intensity at pH 2 is higher than pH 10 and pH 7. To understand the reason behind the increase in intensity at pH 2 and the gradual shift to the right with increase in pH, an excitation scan was performed and a similar result for the intensity at pH 2 was obtained. The excitation curve of pH 2 is comparatively narrower and of sharper than pH 7 and pH 10 (Figure 3.7 b). We hypothesize that the increase in intensity and narrow peak at pH 2 is mainly due to two reasons. Firstly, the hydrophobic environment of the residues at pH 2 results in a blue-shifted emission scan and an increase in intensity and a narrow peak for the excitation scan. Secondly, the RET from the

aromatic amino acids like tyrosine and phenylalanine to tryptophan residues also results in an increase in intensity of the tryptophan peak. However, we observed RET only at pH 2 because the tyrosine residues originally present in the Trp1 mutant are neutralized by the excess H^+ ions, thereby, resulting in an increase in the intensity of the tryptophan residues due to tyrosine to tryptophan RET. Moreover, a conformational change for the Trp1 mutant was observed with increasing pH from 2 to 10. At low pH, the fibers were aggregated and compactly packed, while at high pH, they were more hydrated and dispersed (Figure 3.7 c).

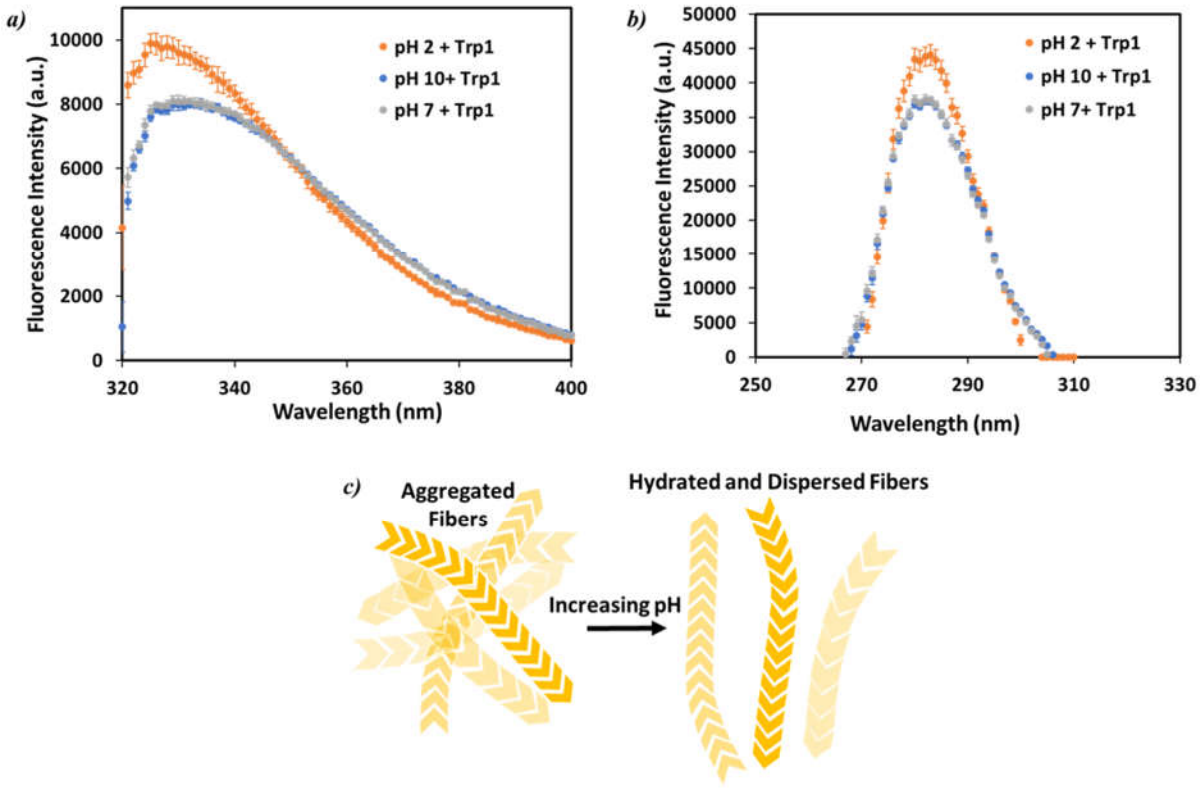

Figure 3.7. Increase in pH results in a spectral shift and changes the environment of the tryptophan residues from hydrophobic to hydrophilic. a) emission scan at 290 nm shows that as the pH increases, the tryptophan residues get exposed to the solvent and a red-shifted spectrum is observed. b) Excitation scan at 330 nm for 0.5 mg/mL Trp1 mutant shows that a narrow and steeper spectrum for pH 2, this indicates a hydrophobic environment around the tryptophan residues. c) Schematic illustration of how increasing pH de-aggregates the protein fibers.

3.3.4.2. Protein Unfolding

The phenomenon of protein unfolding can be observed by using denaturing agents such as GdmCl or urea. Since our curli nanofiber proteins are highly resistant to urea, GdmCl is a useful candidate to observe the unfolding of Trp1 mutant using fluorescence spectroscopy by varying the concentration of GdmCl. Using a spectroscopic technique to analyze the structure by studying the unfolding for our protein is useful because it will help us determine the ideal GdmCl concentration to use for purifying proteins, as we do not want to denature the proteins upon production. It can be observed that the concentration of GdmCl plays an important role in denaturing proteins. By varying the concentration from 0.5 M (after which the proteins were still folded, and the tryptophan residues buried in the hydrophobic environment) to 8 M (above which the proteins are denatured). The high concentration of GdmCl resulted in (partial or complete) disruption of the Trp1 mutant structure, which can be captured in the form of a red-shift to a longer wavelength, thereby further exposing the tryptophan residues to the solvent.

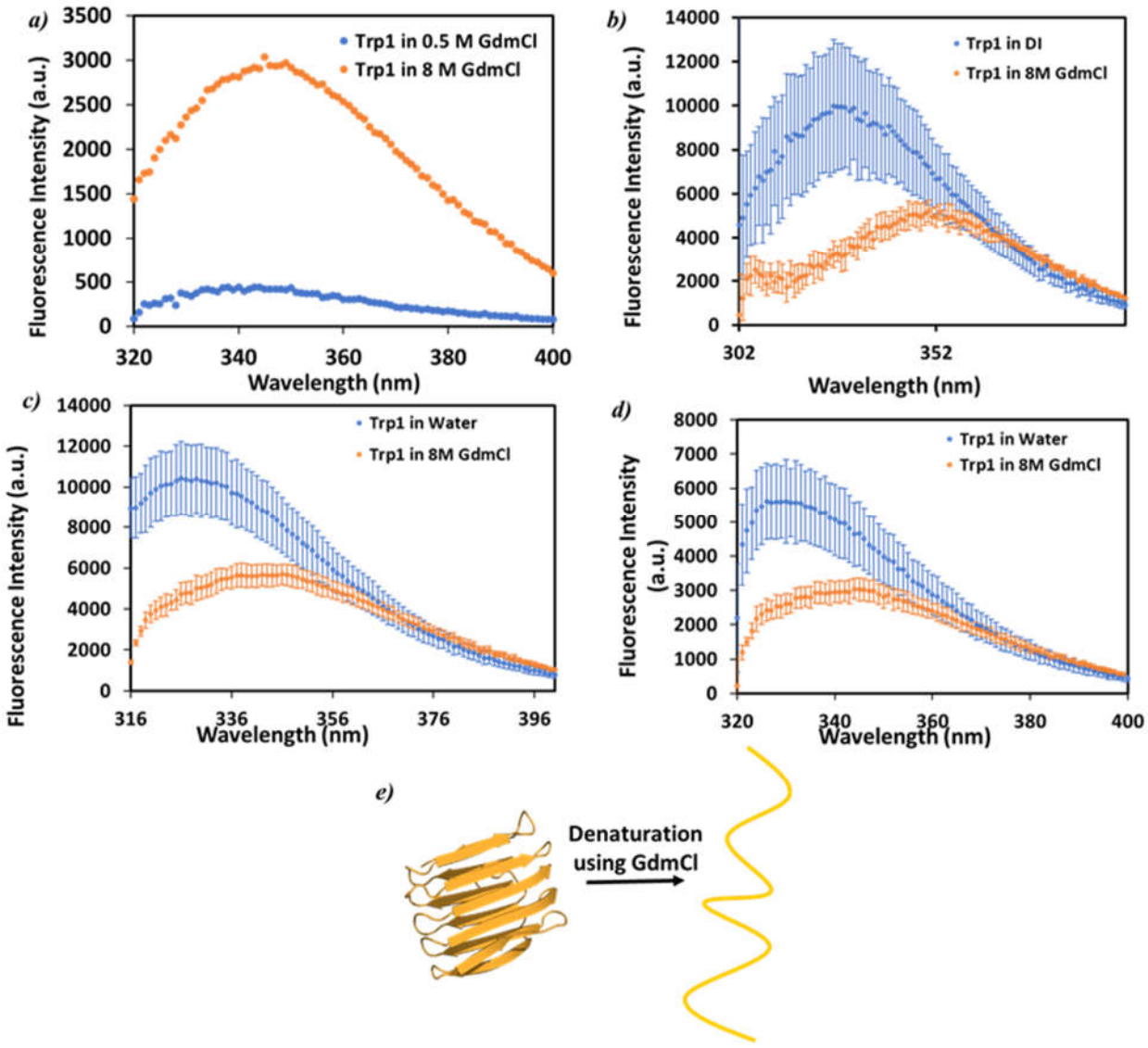

Figure 3.8. Disrupting the protein structure using GdmCl, a denaturing agent, results in a red-shifted spectrum. Fluorescence spectroscopy to understand the conformation of 0.5 mg/ml Trp1 mutant in DI water and 8 M GdmCl when excited at a) 275 nm, b) 290 nm, and c) 295 nm. d) Unfolding of 0.5 mg/ml Trp1 mutant by varying the concentration of GdmCl from 0.5 M to 8 M results in a gradual red-shifted spectrum. Yellow arrows point to the peak of the spectrum e) Schematic representation of protein losing its structure upon being denatured by GdmCl.

3.4. Conclusion

In summary, the β-helix secondary structure for the mutant proteins was confirmed using CD, and the higher content of tryptophan residues was confirmed by Raman spectroscopy and fluorescence

intensity. To gain insight into the π-π stacking between the aromatic rings of the tryptophan residues, fluorescence spectroscopy was performed, and a slight red-shift was observed, suggesting the possibility of π-stacking and electron delocalization through the rings.

Lastly, the environment effect on the tryptophan residues was investigated and it was observed that with increasing pH, the aggregated residues became de-aggregated resulting in a red-shift. A similar effect was observed with the use of denaturing agent GdmCl, an increase in the concentration resulted in unfolding of the protein structure, thereby, causing a red-shifted spectrum.

Ultimately, the aggregation behavior of the fibers could further be linked to their conductivity. Since the fibers aggregate, the five tryptophan residues in each subunit of the Trp1 mutant can result in interactions of the aromatic rings between the subunits. These interactions may contribute to charge delocalization through π-stacking across subunits, and potentially across fibers. Such interactions may then modulate the conductivity levels of the fibers. Understanding when and how fibers aggregate then becomes important for explaining their electrical properties.

3.5. References

1. Hauser, C. A. E. & Zhang, S. Peptides as biological semiconductors. *Nature* **468,** 516–517 (2010).

2. Handbook of Pharmaceutical Controlled Release Technology - Donald L. Wise - Google Books. Available at: https://books.google.ca/books?id=paEzHRHlXE4C&pg=PA86&dq=J+controlled+release&hl=en&sa=X&ved=0ahUKEwi2hfGUm9bZAhUCr4MKHVfYCJ4Q6AEILjAB#v=onepage&q=J controlled release&f=false. (Accessed: 6th March 2018)

3. Ashkenasy, N., Horne, W. S. & Ghadiri, M. R. Design of self-assembling peptide nanotubes with delocalized electronic states. *Small* **2,** 99–102 (2006).

4. Dorval Courchesne, N.-M., Duraj-Thatte, A., Tay, P. K. R., Nguyen, P. Q. & Joshi, N. S. Scalable Production of Genetically Engineered Nanofibrous Macroscopic Materials via Filtration. *ACS Biomater. Sci. Eng.* **3,** 733–741 (2017).

5. Reguera, G. *et al.* Extracellular electron transfer via microbial nanowires. *Nature* **435,** 1098–1101 (2005).

6. Adhikari, R. Y., Malvankar, N. S., Tuominen, M. T. & Lovley, D. R. Conductivity of individual Geobacter pili. *RSC Adv.* **6,** 8354–8357 (2016).

7. Malvankar, N. S. *et al.* Structural basis for metallic-like conductivity in microbial nanowires. *MBio* **6,** e00084 (2015).

8. Dorval Courchesne, N.-M. *et al.* Biomimetic engineering of conductive curli protein films.

Nanotechnology **29,** 454002 (2018).

9. DeBenedictis, E. P., Ma, D. & Keten, S. Structural predictions for curli amyloid fibril subunits CsgA and CsgB. *RSC Adv.* **7,** 48102–48112 (2017).

10. Lakowicz, J. R. *Principles of Fluorescence Spectroscopy Third Edition*. (2006).

11. Dusa, A. *et al.* Characterization of Oligomers during R-Synuclein Aggregation Using Intrinsic Tryptophan Fluorescence †. *Biochemistry* **45,** 2752–2760 (2006).

12. Touchette, J. C., Williams, L. L., Ajit, D., Gallazzi, F. & Nichols, M. R. Probing the amyloid-β(1–40) fibril environment with substituted tryptophan residues. *Arch. Biochem. Biophys.* **494,** 192–197 (2010).

13. WEBER, G. Fluorescence-polarization spectrum and electronic-energy transfer in tyrosine, tryptophan and related compounds. *Biochem. J.* **75,** 335–45 (1960).

Chapter 4 : Electrical Characterization of Self-Healing Tryptophan-mutated Protein Films

In this chapter, we investigated the properties desirable for flexible, stretchable, and self-healing electronics. We studied the effect of different factors, such as film thickness and film hydration, on the conductivity mechanism of tryptophan containing protein films, observed the healing of curli fiber films, and tested whether the electrical properties can be retained upon healing.

4.1. Introduction

Curli nanofibers are self-assembling proteins secreted by *E. coli* bacteria as an extracellular polymeric substance. These proteins can be genetically engineered into conductive nanofibers. Previously, studies have been performed by Kalyoncu *et al.* to incorporate conductivity into the proteins by attaching a functional peptide containing aromatic amino acids at one end of the CsgA monomer. It was observed that tyrosine and tryptophan residues had the highest conductivity, however, the observed conductivity could not provide clear conclusion as the readings were performed using biofilm solutions drop-casted on gold electrodes and even the mechanism of electron transfer was not clear[1]. Another study was performed by Dorval Courchesne *et al.* to incorporate conductivity into curli proteins through genetic engineering in the core of the CsgA monomer. The genetic modifications were performed to detach the biofilm from the surface of the bacteria upon secretion and to position aromatic amino acids in rows within 5 Å of distance for electron delocalization through π-stacking[2]. It was observed that factors such as humidity and surface area effected the conductance results. Research on mutated curli film showed that increase

in humidity resulted in an increase in conductance, and an increase in electrode spacing resulted in increased resistance to the flow of charges[2]. Since the curli films are responsive to changes in environment such as humidity, they could be used as humidity sensors, which can be used in a variety of applications such as solar cells and wearable bioelectronics. Other parameters such as thickness of the film placed on an electrode and effect of drying on the film, have not been studied to understand the conductivity mechanism. Understanding what the effect of drying on the protein structure is, and how thickness of the film effects the current flow is important for developing wearable humidity sensors.

Self-healing materials are metals, polymers, ceramics and composites that have the ability to restore their original properties when damaged via mechanical, thermal or other means[3]. The inflicted damage can be in the form of cracks which can be partially or completely healed during the process[4–7]. Because of their highly desirable characteristic of healing, they are used in a wide range of applications, including solar cells, sensors, biomedical applications, supercapacitors, coatings, adhesives, electronic skin, bioactuators, etc. Due to their growing popularity, an estimated cad $ 2.5 billions investment will be only for the self-healing materials by 2021[8]. Specifically, self-healing electronics are composed of electrically conductive materials that can repair themselves upon any damage in the form of wear and tear. As previously discussed, healing property can be incorporated into materials such as polymers, by mixing a self-healing polymer in the proper ratio without compromising the healing property with a polymer possessing the desired property such as mechanical strength. Some of the mechanisms for healing includes swelling, entanglement of polymer chains, and reversible molecular interactions. For example, Lei *et al.* incorporated calcium carbonate nanoparticles into an alginate polyacrylic acid hydrogel, thereby developing an ionic conductor. Due to the Ca^{2+} ions and the negatively charged chains of alginate

and polyacrylic acid, these hydrogels had self-healing ability. Along with providing the gels with a self-healing ability, Ca^{2+} ions resulted contributed to ionic conduction, and when combined with a dielectric layer, resulted in a self-healable capacitor. Since capacitance in a capacitor is a function of area, this device was used for human motion detection and blood pressure measurements by the changes in the area upon deformation due to damage[9].

Another study performed on an electrically healable material, PEDOT: PSS polymer, showed that a film made of this polymer was electrically conductive before being damaged with a blade, but that a scratch would cause conductivity to drop. The film was able to electrically heal upon addition of water (Figure 4.1). A thickness of more than 1 µm was needed for the polymer to electrically heal on a substrate[10]; therefore, the polymer PEDOT: PSS is not just flexible and electrically conductive but can also be healed electrically.

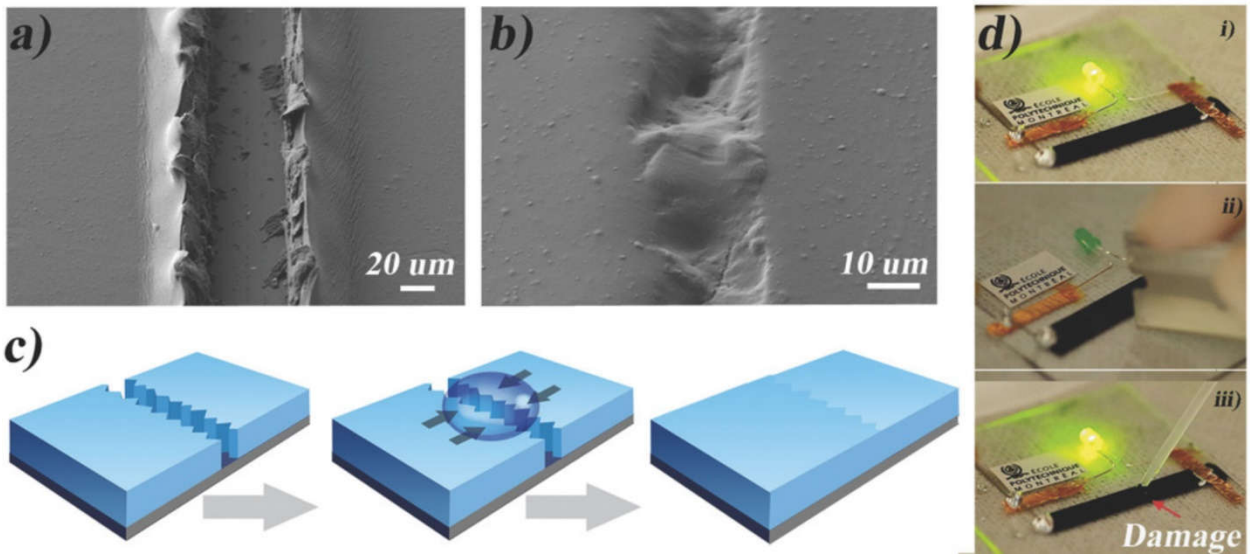

Figure 4.1. Electrical healing is observed in PEDOT: PSS polymer with a drop of water. SEM images a) of the cut, b) after the cut, c) Schematic illustration of the cut and healing process, d) Electrical healing demonstrated using a LED[10], i) It was lit before the cut when the current was flowing through the film, ii) The LED got disconnected when the film was cut, iii) The damaged film was conducting again with a drop of water and the LED lit up.

In this work, taking inspiration from electrical healing studies performed on conductive polymers such as PEDOT: PSS, we wanted to test and demonstrate the healing ability of the mutated curli thin films at the microscopic and macroscopic levels, and test whether the films can retain their electrical properties after healing. As shown in Figure 4.2, free-standing curli films were previously used to build a house-like structure by simply "gluing" the sheets of curli nanofibers together just with the use of water[11]. We hypothesized that water is acting as a "glue" between the sheets by allowing the protein fibers to become mobile and entangle together, thereby making them intact with each other and stick together upon drying.

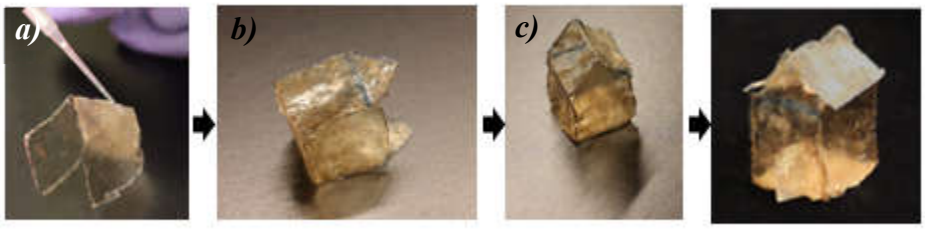

Figure 4.2. Dried thin curli films can be glued together using water, a) water being used to attach thin sheets of curli films, b) dried sheets attached together, c) completed house structure built from curli films using water as the gluing agent[11].

In this chapter, we performed electrical characterization of curli films to understand the properties desirable for flexible, stretchable, and self-healing electronics. In the following sequence, we first investigated how conductivity changes with different environmental parameters and whether we can use these studies to better understand the conductivity mechanism for our curli films. Second, we performed self-healing tests by observing electrical healing in mutant curli films to potentially use them as electrically healable sensors.

4.2. Materials & Methods

4.2.1. Scanning Electron Microscopy (SEM)

5 µl hydrogel was pipetted on 0.5x0.5 cm^2 glass slides to image the self-healing of the fibers. These samples were washed with 0.1 M sodium cacodylate buffer and then fixed with 2% glutaraldehyde and 2% paraformaldehyde. The samples were then washed in water bath followed by ethanol baths for 15 minutes with gradually increasing concentration of ethanol (25%, 50 %, 75 %, 100%(v/v)). Samples were then dried using Leica Microsystems EM CPD030 Critical Point Dryer and sputter coated using Leica Microsystems EM ACE600 High Resolution Sputter Coater with a 5 nm layer of Pt. SEM imaging was performed using FEI Inspect F50 FE-SEM.

4.2.2. Electrical Characterization

Hydrogels of Trp1 mutant and WT were produced by vacuum filtration protocol using GdmCl, SDS (5%) and benzo nuclease to obtain pure proteins from the large-scale culture. The electrodes were printed using Voltera V-One circuit printer. Silver ink (<90% silver, Voltera) was used for printing the electrodes on the substrate. Glass slides used as substrates for the electrodes were purchased from Fisher Scientific. The glass slides were first cleaned using soap water, acetone, and isopropanol with sonication for 10 minutes between each step, before printing silver electrodes onto them. The electrodes printed had dimensions of 3 mm in length and 1 mm in width. Scotch tape was placed along the width of the electrode to create a window of dimensions 3x1 mm to restrict the hydrogel within the window (Figure 4.3). Razor blades (product number: 9412071) used for scratching the dried films were purchased from Fisher scientific. DI water was used for healing the scratched film and was supplied by the reverse osmosis system. All the electrical characterizations were performed using a Keysight B1500A Semiconductor Device Analyzer

which was connected to an Everbeing C-2 probe station placed inside a shielding box and on an antivibration table. Electrical

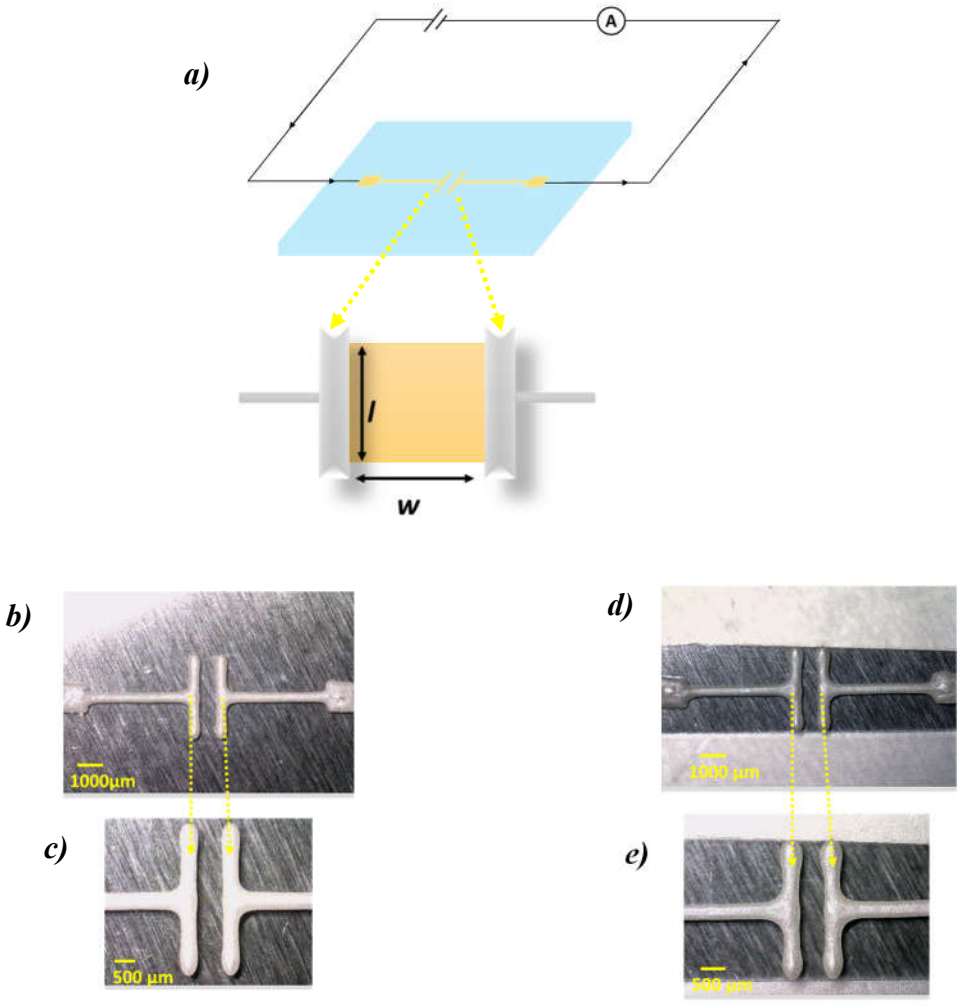

Figure 4.3. Silver electrodes were printed on a glass substrate with dimensions of the window 3x1 mm as the length (l) and width (w) of the electrode respectively, a) Schematic representation of measurement setup and a higher magnification drawing of the electrode, b-c) Optical microscope images of silver electrodes without window and a higher magnification image, d-e) Optical microscope images of the electrodes with a window and a higher magnification image of the window.

contacts with the silver electrodes were established using two probes touching the electrodes on both the sides of the dried film. The thickness of these films was measured using Dektak XT profilometer by Bruker with 1 mg stylus force using 25 µm diameter stylus tip.

Determining thickness and resistance correlation: Hydrogel was drop-casted onto the electrodes printed on a glass slide. The amount of hydrogel drop-casted onto each electrode was sequentially increased by increments of 4 μL to obtain different film thicknesses. The hydrogels were then allowed to dry at room temperature in ambient air at 47% RH (measured using humidity meter) for 20 minutes. Electrical measurements were performed, and the film resistance was obtained from the slope of the I-V graphs.

Effect of hydrogel drying with time: 4 μL Trp1 mutant hydrogel was drop-casted onto the silver electrodes and I-V measurements were taken from -5 to 5 V every minute from time 0 to 40 minutes to monitor drying. The hydrogel had a neutral pH of 6.5-7 and was used directly after vacuum filtration.

Scratch and rehydration test: Electrical measurements were performed after each step of scratch and hydration test. Dried films were obtained by gently drop-casting 4 μL hydrogel thin films on to the glass substrates. These were dried at room temperature for 20 minutes at 47% RH. The dried films were then gently scratched using a razor blade, followed by drop-casting 2 μL DI water on the scratched surface and allowing it to dry for 20 minutes.

4.3. Results & Discussion

4.3.1. Conductivity Mechanism

4.3.1.1. Effect of thickness on resistance

The effect of thickness on resistance was tested to determine whether fabricating thicker protein films would result in higher current, or whether charge transport at the electrode surface dominates. A set of 10 silver electrodes were printed on a glass substrate both for WT and Trp1

mutant. Different volumes of hydrogels were drop-casted onto the electrodes and allowed to dry. I-V measurements were performed for each film of different thickness and the conductance was obtained from the slope of I-V graphs.

$$Conductance = slope\ of\ the\ I - V\ graph \qquad (1)$$

The thickness for each film measurements was performed using a profilometer. From Figure 4.4 a-b, it can be observed that for this electrode configuration as the thickness of the film for both Trp1 mutant and WT increases, the conductance increases (resistance decreases) which means that charge transport is occurring throughout the bulk of the film rather than only at the electrode surface. If the charge transport was only a surface phenomenon limited, then we would not have obtained a linear correlation between thickness and conductance.

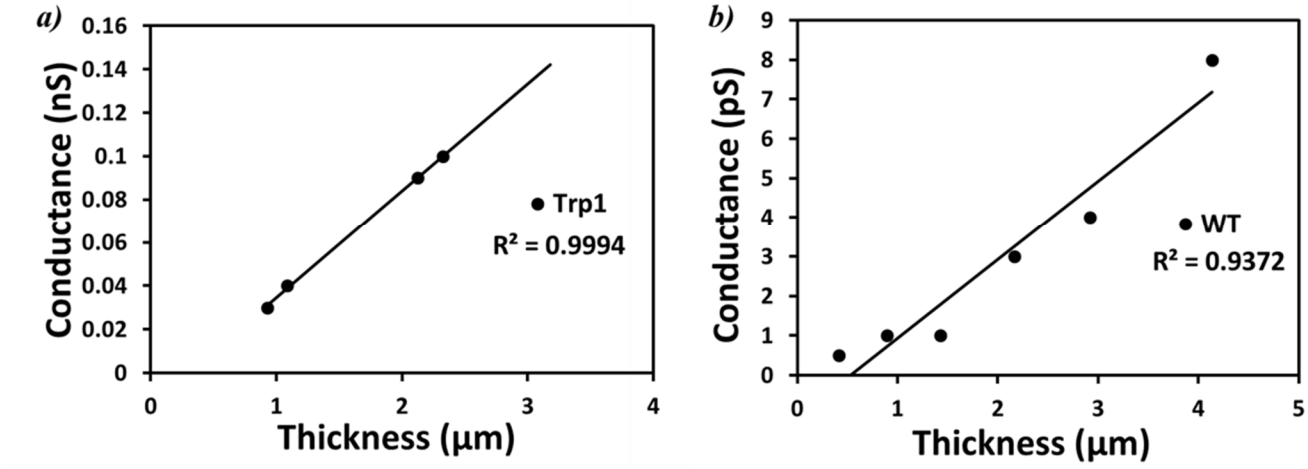

Figure 4.4. With an increase in thickness conductance through the Trp1 mutant and WT films increases, indicating that charge flow occurs throughout the bulk of the film rather than just the surface. a) Conductance of the Trp1 mutant and b) WT thin film were observed with increasing thickness. Thickness was measured using profilometer using 1 mg stylus force with 25 µm diameter stylus tip.

4.3.1.2. Hydrogel Drying with time

To better understand the effect of humidity and drying on the electrical properties of the Trp1 mutant film, a relationship between current and drying time was established. It was observed that, as the film dries with time, the current flow through the film decreases down to a certain value and then fluctuates around that value (Figure 4.5 c-d). We hypothesize that water is necessary for

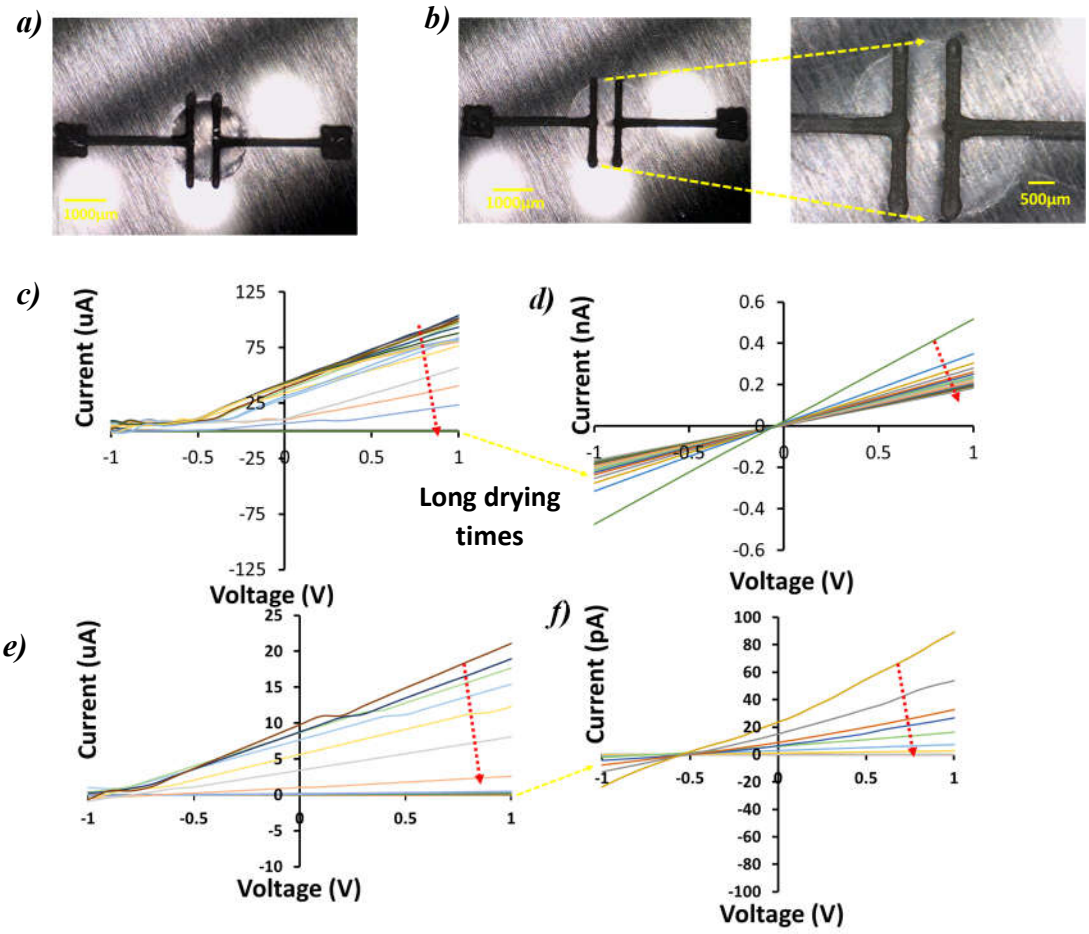

Figure 4.5. Conductance decreases with time as the hydrogel dries with time into thin film, a) Trp1 mutant hydrogel drop-casted onto the silver electrodes, b) Trp1 mutant thin film after 20 minutes of drying. I-V measurements taken for Trp1 mutant hydrogel from 0 to 40 mins (c) and WT hydrogel from 0 to 40 mins (e) to observe the decrease in current at 1 V. d, f) I-V measurements from 19 to 40 mins for Trp1 mutant (d) and WT (f) when the films dried.

proper protein configuration in order for charges to flow and when the film is dry, the protein structure does not support proper flow of charges. The drying process of the hydrogel can be

observed from the I-V measurement of Trp1 mutant, which shows a decrease in slope over time, i.e., decreasing conductance with time (Figure 4.6 e). However, constant high voltage application can be a source of error as it can result in decrease in current due to drying of the fibers**.** We arbitrarily selected 20 minutes as the drying time for consistency of our subsequent measurements as the current dropped from µA to nA at this point, indicating that the surface water has dried leaving behind a thin film with fine layer of water in the bulk.

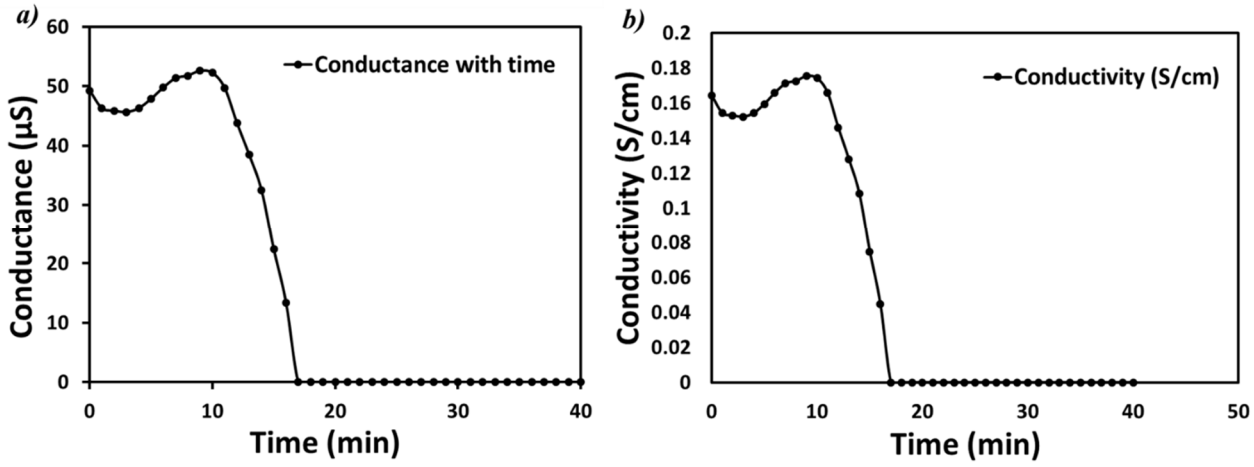

Figure 4.6. a) Conductance-time graph plotted from the graphs c and d in Figure 4.5. As the film starts to dry, the conductance decreases and there is a sharp decrease after the 19th minute when the water content of the hydrogel has evaporated, b) Conductivity-drying time response at 5 V to hydrogel drying into the thin film. The conductivity was calculated by using the conductance values from Figure 4.5 e. Most of the water content from the hydrogel had dried and it can be observed that as the hydrogel dries with time, there is a decrease in current and therefore the conductivity.

4.3.2. Testing Visible Healing

To observe healing at the microscopic level, scanning electron microscopy (SEM) was performed. A sample of hydrogel was drop-casted onto three 0.5 cm x 0.5 cm glass substrate and allowed to dry into a thin film at room temperature. Two of the three dried films were scratched using a blade and then a drop of water was placed on one of the scratched films and allowed to dry to test for visible healing. A schematic illustration of the entire process is shown in Figure 4.7 a.

We saw that when the original film was scratched with a minimum width of 80 µm, the scratched film could be healed by using water (Figure 4.7 b-d). The fibers would become mobile and entangle themselves, thereby resulting in healed film.

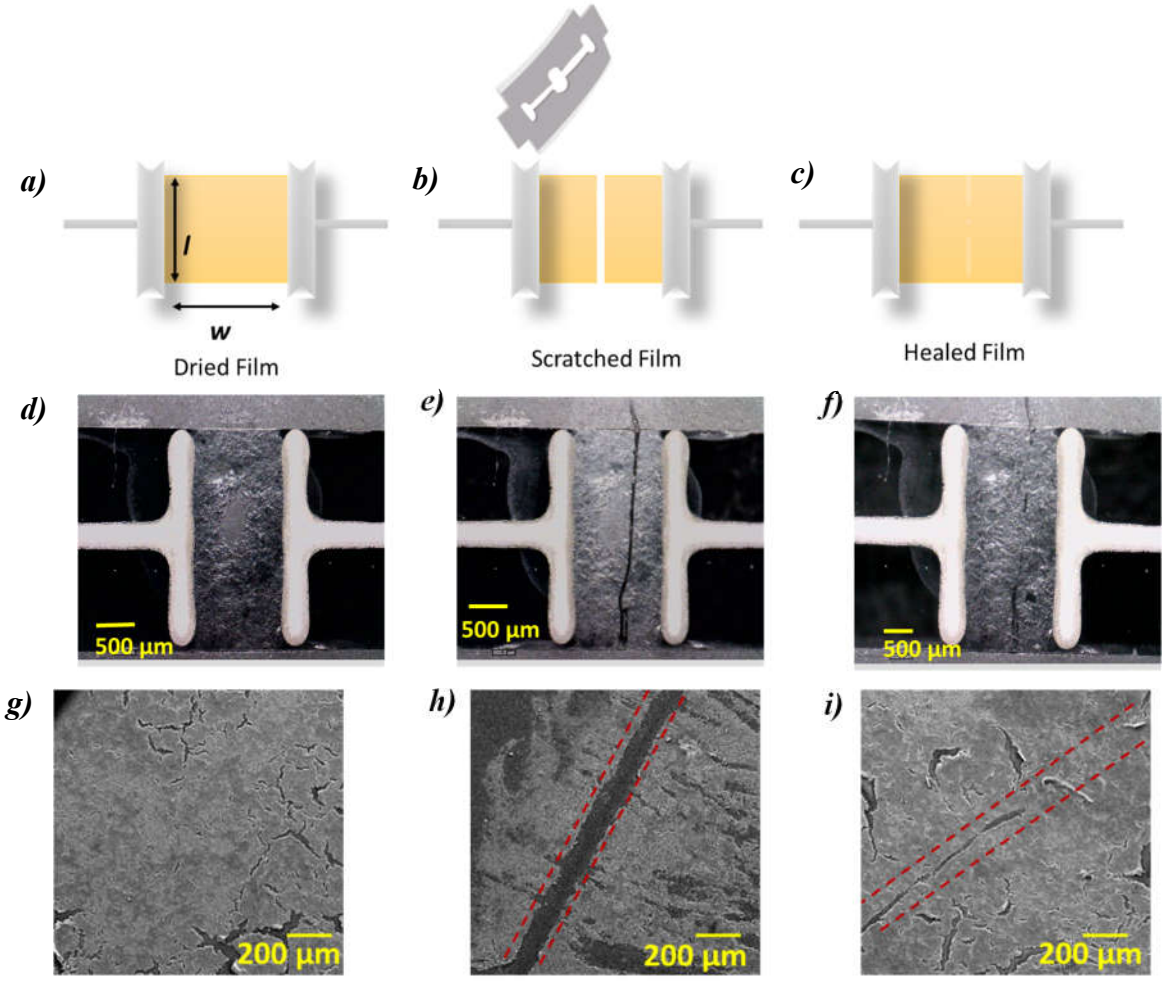

Figure 4.7. Curli fiber thin films can be healed using water. Schematic illustration of scratch and rehydration test, optical microscope and SEM images of dried film (a, d, g), scratched film (b, e, h) and healed film (c, f, i). For optical microscope images, hydrogel was drop-casted into the window and allowed to dry before inflicting a scratch followed by healing using water. For SEM images, hydrogel was drop-casted onto three 0.5 cm x 0.5 cm glass slide and allowed to dry. Two of them were then cut with a razor blade and only one with the cut was treated with water.

The effect of thickness on self-healing of the film was also studied and it was observed that films as thin as 0.5 µm could easily be healed for a maximum 80 µm width cut, i.e., a very thin

film of 0.5 µm thickness could easily be healed even if the cut was 80 µm wide. We hypothesized that the healing of the curli nanofibers films is due to the swelling of the fibers upon hydration with water, which makes them mobile enough to cross over the gap and entangle together thereby, healing the damage (Figure 4.7 f).

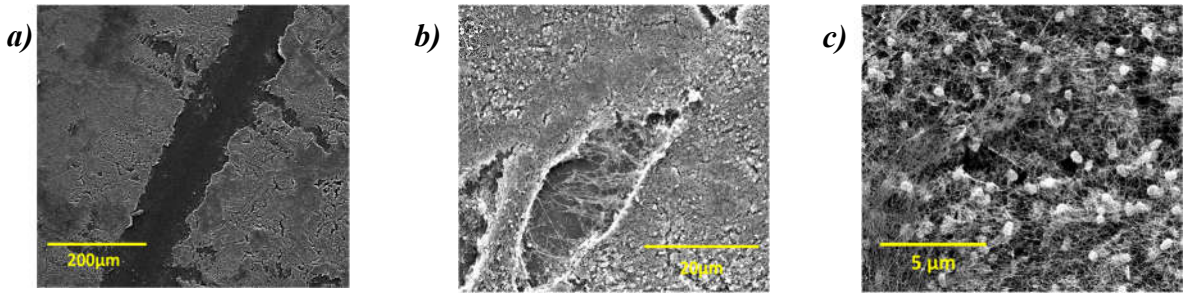

Figure 4.8. SEM images at h) higher magnification of the cut film of width 150 µm, i) Fibers crossing over the cut gap and beginning to heal, j) Further magnification showed mesh of protein fibers upon healing.

4.3.3. Electrical Characterization

Conductive curli hydrogels were obtained directly from vacuum filtration and were drop-casted onto silver electrodes which were printed on a glass substrate. A thin film of curli nanofibers was used to demonstrate the self-healing phenomena at the micro level. A gentle cut was made on the film using a blade to demonstrate the self-healing property of the film. Damage to the film in the form of a vertical cut resulted in a gap in the film, thereby hindering the flow of current across the film (Figure 4.7 e-f). Coating the scratched film with a drop of water resulted in healing the film within 20 minutes of drying the film. Interestingly, a single cut or multiple cuts on the same film, of width as large as 80 µm, could be healed within the same time span, in this case 20 minutes of drying with just a drop of water. The above process was not just reproducible but also very reliable as both Trp1 mutant and WT showed self-healing when the scratched films were covered with a drop of water.

It was observed that a Trp1 mutant thin film (as thin as 0.5 μm) had an electrical conductivity of 119.3 nS/cm, compared to the WT curli nanofiber thin film (the control) which had an electrical conductivity of 90.96 nS/cm. There was electrical healing observed for both the curli nanofiber thin films, Trp1 and WT, by simply covering the scratched film with a drop of water and allowing it to dry. The thin films were healed upon drying for 20 minutes and their electrical properties were restored. These mutated curli films are known to be conductive[2], mouldable, and freestanding[11]. Furthermore, the electrical healing property along with the mechanical strength of the dried films makes them highly suitable for applications in electronic skin, wearable sensors, and self-healing electronics.

4.3.3.1. Water-Induced Electrical Healing

To show that not just visibly but also electrically successful healing of the films has occurred, current-voltage (I-V) measurements were performed before and after scratching and healing. It can be seen from Figure 4.9, that Trp1 mutant and WT healed electrically by comparing the current at 5 V after being scratched and after being healed with a drop of water upon drying. To elaborate more, the Trp1 mutant and WT films with the cut had no current flow because of the gap created due to the damage. The films before the damage had the highest current, followed by films after healing. Moreover, our findings on the magnitude of current from I-V measurements for the dried Trp1 mutant in nanoampere (nA) and WT in picoampere (pA) are consistent in magnitude with the previously established data[2]. It is important to emphasize here that the films of thickness as low as 0.5 μm not just healed visibly, but also electrically. Curli fiber films therefore require a thinner layer to heal compared with PEDOT: PSS films which required minimum thickness of 1 μm to electrically heal[10].

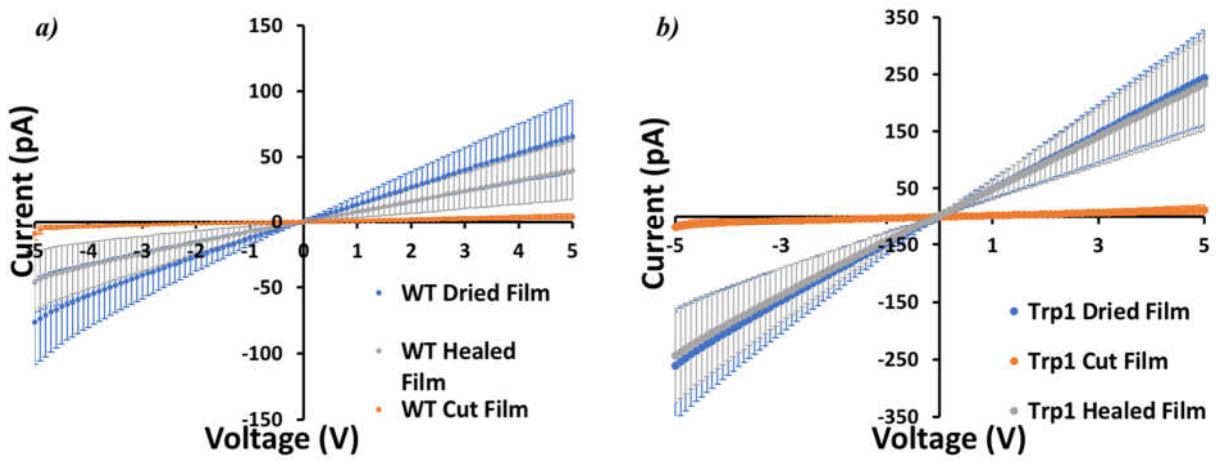

Figure 4.9. Curli fiber thin films can be electrically healed. Electrical healing observed in a) Trp1 mutant and b) WT thin film when it was scratched with a razor blade and a drop of water was placed over the cut to heal. Electrical measurements were made after drying, scratching and healing the thin film.

4.4. Conclusion

In order to gain insight into the conductivity mechanism of Trp1 mutant and WT, a series of experiments were performed. We hypothesize that charge transport occurs not just on the surface but also throughout the bulk of the film as a linear correlation was observed between the thickness and conductance of the film. If the charge transfer was surface limited, then we would not see a linear increase in conductance with an increase in thickness. Furthermore, we hypothesize, from the drying of hydrogel experiment, that hydrated films resulted in proper protein structure for flow of charges through the bulk of the film. Based on the above-mentioned observations, there is a possibility of dual conduction mechanisms (electronic and ionic). However, the ionic conduction dominates over electronic conduction in the presence of moisture or when the film is hydrated.

Genetically modified mutant films show a 20% increase in conductance compared to WT. The reproducibility of the I-V results for dried Trp1 mutant film show that the conductance observed belonged to the protein itself (and its aromatic residue content), and not to other factors like water. These films were not just conducting, but also self-healing by swelling and re-entanglement of disconnected fibers using a drop of water, upon an inflicted scratch. A successful electrical healing with more than 90 % recovery was observed for Trp1 mutant. Since our mutant curli films can be electrically healed using water and are also responsive to humid environment, they could be used for making self-healing humidity sensors.

4.5. References

1. Kalyoncu, E., Ahan, R. E., Olmez, T. T. & Safak Seker, U. O. Genetically encoded conductive protein nanofibers secreted by engineered cells. *RSC Adv.* **7,** 32543–32551 (2017).

2. Dorval Courchesne, N.-M. *et al.* Biomimetic engineering of conductive curli protein films. *Nanotechnology* **29,** 454002 (2018).

3. Wool, R. P. Self-healing materials: a review. *Soft Matter* **4,** 400 (2008).

4. Ge, T., Pierce, F., Perahia, D., Grest, G. S. & Robbins, M. O. Molecular Dynamics Simulations of Polymer Welding: Strength from Interfacial Entanglements. *Phys. Rev. Lett.* **110,** 098301 (2013).

5. Hentschel, J., Kushner, A. M., Ziller, J. & Guan, Z. Self-Healing Supramolecular Block Copolymers. *Angew. Chemie Int. Ed.* **51,** 10561–10565 (2012).

6. Chen, Y., Kushner, A. M., Williams, G. A. & Guan, Z. Multiphase design of autonomic self-healing thermoplastic elastomers. *Nat. Chem.* **4,** 467–472 (2012).

7. Chen, X. *et al.* A thermally re-mendable cross-linked polymeric material. *Science* **295,** 1698–702 (2002).

8. Self-Healing Materials Market by Form (Extrinsic, Intrinsic), Material Type (Concrete, Coatings, Polymers, Asphalt, Ceramic, Metals), End-Use Industry (Building & Construction, Transportation, Mobile Devices), and Region - Global Forecast to 2021. Available at: https://www.researchandmarkets.com/reports/4109810/self-healing-materials-market-by-form-extrinsic. (Accessed: 29th July 2019)

9. Lei, Z., Wang, Q., Sun, S., Zhu, W. & Wu, P. A Bioinspired Mineral Hydrogel as a Self-Healable, Mechanically Adaptable Ionic Skin for Highly Sensitive Pressure Sensing. *Adv. Mater.* **29,** 1700321 (2017).

10. Zhang, S. & Cicoira, F. Water-Enabled Healing of Conducting Polymer Films. *Adv. Mater.* **29,** 1703098 (2017).

11. Duraj-Thatte A.§, Manjula-Basavanna A.§, Dorval Courchesne N.-M.§, Cannici G., Sanchez-Ferrer A., Frank B.P., van't Hag L., Fairbrother H., Mezzenga R., J. N. S. . Water-Processable, Biodegradable and Coatable Aquaplastic from Engineered MicrobialBiofilms. *Nat. Chem. Biol.* (submitted).

Chapter 5: Conclusion

In conclusion, the curli nanofiber mutant Trp1 was analysed structurally, electrically and tested for the ability to self-heal. The β-sheet secondary structure of the proteins, as well as the high concentration of tryptophan residues in the Trp1 mutant, were confirmed via Raman and fluorescence spectroscopy. Most importantly, the structural analysis of Trp1 mutant and random Trp mutant through fluorescence spectroscopy helped us gain insights towards the possibility of the π-stacking of the aromatic rings in the Trp1 mutant, which contributes in the delocalization of electrons between the tryptophan residues. Further structural analysis done using fluorescence spectroscopy, resulted in a peak shift to the right with 330 nm as the reference representing aggregated protein structures. This shift implied protein de-aggregation by increasing the pH and protein denaturation by increasing the concentration of GdmCl in the solution. Finally, due to the well-defined tryptophan fluorescence emission peak, the Trp1 mutant proteins could be used as a candidate for making a FRET sensor in combination with a dye.

For electrical characterization, factors affecting the conductance results such as drying, and thickness of the protein films were studied. Firstly, an increase in thickness resulted in an increase in conductance of the film. It was concluded that charge transport is both a bulk and surface phenomena and therefore, a relationship between thickness and conductance was observed. Secondly, conductance decreased with increasing drying time. This observation indicates that water contributes in maintaining the protein structure needed for the charges to flow through the protein film. In order to understand the contribution of protons in the conductivity of curli fibers, using D_2O instead of water when hydrating films for electrical measurements is recommended.

Since D_2O does not contain protons, the expected I-V results should be lower than the I-V results obtained using H_2O.

Further, successful visible self-healing was observed for WT and Trp1 mutant films. Electrical characterization was performed to observe electrical-healing. It was observed that thin films made of mutant Trp1 fibers had higher conductivity compared to WT, and that the protein films demonstrated successful electrical self-healing. Trp1 mutant curli films were concluded to heal electrically by adding a drop of water onto a scratch to allow for the film to reform. A recovery of over 95 % of initial conductivity value was observed. In the future, further studies can be performed to better understand the self-healing behavior of the protein films, including understanding the effect of ambient humidity on the self-healing of the films, and determining the effects of cut size and film thickness on water-induced healing. Since free-standing curli films can be attached together physically and can self-heal both visibly and electrically, they could further be used to fabricate composites by combining them with polymers or nanomaterials for use in bio-electronic applications.

Overall, curli fibers represent a novel class of protein scaffolds that could be used to fabricate biodegradable, non-toxic, genetically-customizable conductive materials. The protein production can easily be scaled up to produce materials that response to environmental changes. The self-healing abilities of conductive curli thin films observed here, as well as their response to humidity, indicate that curli fibers could be used for a range of applications: from wearable and flexible films, to self-healing devices, and humidity sensors.